Available online at www.sciencedirect.com
ScienceDirect
Journal of Computational Physics 222 (2007) 194–216
JOURNAL OF COMPUTATIONAL PHYSICS
www.elsevier.com/locate/jcp

Analysis of numerical errors in large eddy simulation using statistical closure theory

Noma Park, Krishnan Mahesh *

Department of Aerospace Engineering and Mechanics, University of Minnesota, 110 Union Street SE, 107 Akerman Hall, Minneapolis, MN 55455, United States

Received 28 March 2006; received in revised form 8 June 2006; accepted 18 July 2006
Available online 1 September 2006

Abstract

This paper develops a dynamic error analysis procedure for the numerical errors arising from spatial discretization in large-eddy simulation. The analysis is based on EDQNM closure theory, and is applied to the LES of decaying isotropic turbulence. First, the effects of finite-differencing truncation error, aliasing error and the dynamic Smagorinsky model are independently considered. The time-evolution of kinetic energy and spectra predicted by the analysis are compared to actual LES using the Navier–Stokes equations, and good agreement is obtained. The analysis is then extended to simultaneously consider all sources of error in a second-order discretely energy conserving, central-difference LES solver. Good agreement between the analysis and actual LES is obtained. The analysis is used to compare the contribution of the subgrid model to that of numerical errors, and it is shown that the contribution of the subgrid scale model is much higher than the numerical errors. The proposed one-dimensional EDQNM-LES model shows potential as a more general tool for the analysis of numerical error, and SGS model in simulations of turbulent flow.

Keywords: Large eddy simulation; Numerical error; EDQNM theory

1. Introduction

Large eddy simulation (LES) appears to be a promising tool for the simulation of complex flows of engineering importance [1–3]. Most LES of complex flows use low order (typically second order) finite difference/volume methods for spatial discretization. An important concern when using finite difference/volume methods in LES, is whether the subgrid scale (SGS) model can function as intended, in the presence of the numerical error. Unlike DNS, flow at the smallest resolved scales in LES is still energetic. As a result, LES solutions are more sensitive to numerical errors than DNS. Therefore, the analysis and control of numerical errors in LES have been investigated by a number of workers [4–12].

* Corresponding author. Tel.: +1 650 725 1821; fax: +1 650 723 9617.
E-mail address: mahesh@aem.umn.edu (K. Mahesh).

0021-9991/$ - see front matter
doi:10.1016/j.jcp.2006.07.016

An error analysis by Ghosal [6] suggests that numerical errors in LES can completely mask the subgrid-scale model (SGS) contribution. Ghosal's analysis considers isotropic turbulence, and compares the power spectral densities of the error terms to the "exact" SGS force in the discrete Navier–Stokes equations. The turbulence is assumed to follow the von Kármán energy spectrum, and the joint normal hypothesis [13] is applied. We will refer to Ghosal's methodology as "static error analysis", since it does not consider the time-evolution of the solution, and characterizes errors by their own statistical measure. Such comparison of the power spectra shows that finite differencing error is the dominant error for low-order schemes, which overwhelms the SGS force at all wavenumbers. Aliasing error is dominant for high-order schemes. Ghosal showed that this conclusion holds regardless of cutoff wavenumber, and proposed explicit filtering technique as a remedy to avoid contamination of the solution. Ghosal's analysis has inspired subsequent studies on the analysis of numerical errors in LES [9,11,12].

Numerical errors in turbulent channel flow were considered by Kravchenko and Moin [7], who used a spectral numerical method, and replaced physical wavenumbers in the derivative operators with modified wavenumbers [22] to approximate the effect of numerical error. This work concluded that for low-order finite-difference schemes, the high wavenumber part of the spectrum, could be adversely affected by truncation error, which could reduce the relative contribution of the subgrid model.

Ghosal's results raise the possibility that low order schemes may not be suitable for LES. However, many successful LES have been reported using low order (not higher than fourth order) finite difference/volume schemes (e.g. [5,12,14–16]). A theory which can predict results obtained from actual LES is therefore required. Development of such a theory is pursued in this paper. An approach similar to [7] is used to introduce numerical error in a spectral LES code for isotropic turbulence. Predictions of kinetic energy decay, and energy spectra from the LES code are used to validate the proposed theory.

A missing element in the static error analysis is the dynamic interaction between numerical errors, the SGS term and the solution. A dynamic theory should at the very least, involve a transport equation for a physical quantity and a reliable theoretical closure. This paper uses the kinetic energy transport equation in wave space; i.e. the energy spectrum evolution equation, to model the dynamic evolution. The nonlinear term is then closed using the eddy-damped quasi-normal Markovian (EDQNM) theory [17,18]. The EDQNM theory has been developed for the Navier–Stokes equations; this paper extends it to the LES equations using the dynamic Smagorinsky model, in the presence of numerical error. Since we solve for the energy spectrum, the analysis is one-dimensional in space. Since the notion of modified wavenumber is used to model numerical error, the analysis is general in the choice of spatial discretization. We consider Fourier, and second-order, staggered grid energy-conserving disretizations in this paper. After validation against actual LES, the analysis is used to compare the magnitude of the subgrid contribution to that of numerical error. This comparison suggests a possible justification for the use of low-order, discretely energy conserving schemes in LES.

The objectives of the present study are therefore, to develop a theoretical model that closely mimics the actual LES system, and to perform a dynamic analysis of numerical errors using the developed theoretical model. The paper is organized as follows. In Section 2, theoretical background and numerical methods are outlined, where EDQNM closure theory is introduced and extended to LES equations adopting SGS model. Numerical errors are incorporated in the kinetic energy transport equation in the wavespace in Section 3. As a result, a simple one-dimensional model for the LES code with second order central difference is established. The results from error analysis are shown in Section 4. In Section 5, the difference between the present analysis and the static error analysis will be highlighted. The paper concludes with a brief summary in Section 6.

2. Theoretical background

2.1. EDQNM closure

EDQNM theory is discussed in detail in [17,18]. Here, we provide a brief summary in the interests of clarity. Consider isotropic turbulence in a cubical box Ω of side L, which obeys the incompressible Navier–Stokes equations,

$$\frac{\partial u_i}{\partial t} = -\frac{\partial}{\partial x_j}(u_i u_j) - \frac{\partial p}{\partial x_i} + \nu \frac{\partial^2 u_i}{\partial x_j \partial x_j}, \quad \frac{\partial u_i}{\partial x_i} = 0. \tag{1}$$

Here, $\mathbf{u} = (u_1, u_2, u_3)$ is the solenoidal vector field, ν is the molecular viscosity and p is the pressure divided by density. Throughout this paper, the summation convention is applied to repeated indices unless otherwise specified. For the convenience of analysis, assume infinite space, or $L \to \infty$. The Fourier coefficient,

$$\hat{u}_i(\mathbf{k}, t) = \frac{1}{8\pi^3} \int_\Omega u_i(\mathbf{x}, t) \exp(-\mathrm{i}\mathbf{k} \cdot \mathbf{x}) \, \mathrm{d}\mathbf{x}, \tag{2}$$

where $\mathbf{k} \in \mathbb{R}^3$ is the wavevector. This implies that

$$\frac{\partial \hat{u}_i(\mathbf{k}, t)}{\partial t} = -\mathrm{i} P_{imn}(\mathbf{k}) \left[\int \int \mathrm{d}^3\mathbf{p} \, \mathrm{d}^3\mathbf{q} \, \delta(\mathbf{p} + \mathbf{q} - \mathbf{k}) \hat{u}_m(\mathbf{p}, t) \hat{u}_n(\mathbf{q}, t) \right] - \nu k^2 \hat{u}_i(\mathbf{k}, t), \tag{3}$$

where δ is the Dirac delta function, $k^2 = k_i k_i$, $P_{imn} = (k_n P_{im} + k_m P_{in})/2$ and

$$P_{ij}(\mathbf{k}) = \delta_{ij} - \frac{k_i k_j}{k_l k_l} \tag{4}$$

is the projection tensor onto the plane perpendicular to $\mathbf{k}$.

Multiplying (3) with $\hat{u}_i(\mathbf{k})^* = \hat{u}_i(-\mathbf{k})$ and taking the ensemble average, yields the transport equation for the energy spectrum $E(k) = 2\pi k^2 \langle \hat{u}_i(\mathbf{k}) \hat{u}_i^*(\mathbf{k}) \rangle$:

$$\left(\frac{\partial}{\partial t} + 2\nu k^2 \right) E(k) = 4\pi k^2 M_{ijm}(\mathbf{k}) \int \int [\mathrm{d}^3\mathbf{p} \, \mathrm{d}^3\mathbf{q} \, \delta(\mathbf{p} + \mathbf{q} - \mathbf{k}) \times \langle \hat{u}_i(-\mathbf{k}) \hat{u}_j(\mathbf{p}) \hat{u}_m(\mathbf{q}) \rangle], \tag{5}$$

where $\langle \, \rangle$ denotes the ensemble and spherical shell average, $(\,)^*$ is the complex conjugate, and $M_{ijm}(\mathbf{k}) = -\mathrm{i} P_{ijm}(\mathbf{k})$. $T_{ijm}(\mathbf{k}, \mathbf{p}, \mathbf{q}) \equiv \langle \hat{u}_i(-\mathbf{k}) \hat{u}_j(\mathbf{p}) \hat{u}_m(\mathbf{q}) \rangle$ is given by its transport equation [19]:

$$\begin{aligned} \left[\frac{\partial}{\partial t} + \nu(k^2 + p^2 + q^2) \right] T_{ijm} = {} & M_{inl}(-\mathbf{k}) \int \int \mathrm{d}^3\mathbf{r} \, \mathrm{d}^3\mathbf{s} \, \delta(\mathbf{r} + \mathbf{s} + \mathbf{k}) \times \langle \hat{u}_j(\mathbf{p}) \hat{u}_m(\mathbf{q}) \hat{u}_n(\mathbf{r}) \hat{u}_l(\mathbf{s}) \rangle + M_{jnl}(\mathbf{p}) \\ & \times \int \int \mathrm{d}^3\mathbf{r} \, \mathrm{d}^3\mathbf{s} \, \delta(\mathbf{r} + \mathbf{s} - \mathbf{p}) \times \langle \hat{u}_i(-\mathbf{k}) \hat{u}_m(\mathbf{q}) \hat{u}_n(\mathbf{r}) \hat{u}_l(\mathbf{s}) \rangle + M_{mnl}(\mathbf{q}) \\ & \times \int \int \mathrm{d}^3\mathbf{r} \, \mathrm{d}^3\mathbf{s} \, \delta(\mathbf{r} + \mathbf{s} - \mathbf{q}) \times \langle \hat{u}_j(\mathbf{p}) \hat{u}_i(-\mathbf{k}) \hat{u}_n(\mathbf{r}) \hat{u}_l(\mathbf{s}) \rangle. \end{aligned} \tag{6}$$

The quadruple nonlinear terms on the r.h.s. of (6) introduce a closure problem which is resolved by introducing the quasi-normal assumption [6,18]:

$$\begin{aligned} \langle \hat{u}_i(\mathbf{p}) \hat{u}_j(\mathbf{q}) \hat{u}_m(\mathbf{r}) \hat{u}_n(\mathbf{s}) \rangle = {} & \delta(\mathbf{p} + \mathbf{q}) \delta(\mathbf{r} + \mathbf{s}) \Phi_{ij}(\mathbf{q}) \Phi_{mn}(\mathbf{s}) + \delta(\mathbf{p} + \mathbf{r}) \delta(\mathbf{q} + \mathbf{s}) \Phi_{im}(\mathbf{r}) \Phi_{jn}(\mathbf{s}) \\ & + \delta(\mathbf{p} + \mathbf{s}) \delta(\mathbf{q} + \mathbf{r}) \Phi_{in}(\mathbf{s}) \Phi_{jm}(\mathbf{r}), \end{aligned} \tag{7}$$

where $\Phi_{ij}(\mathbf{k}) = Q(k) P_{ij}(\mathbf{k}) \equiv E(k) P_{ij}(k)/(4\pi \, k^2)$. Applying (7) to (6) yields

$$\begin{aligned} \left[\frac{\partial}{\partial t} + \nu(k^2 + p^2 + q^2) \right] T_{ijm} = {} & 2\delta(\mathbf{p} + \mathbf{q} - \mathbf{k}) \{ M_{jnl}(\mathbf{p}) P_{in}(\mathbf{k}) P_{ml}(\mathbf{q}) \times Q(k) Q(q) \\ & + M_{mnl}(\mathbf{q}) P_{in}(\mathbf{k}) P_{jl}(\mathbf{p}) Q(k) Q(p) - M_{inl}(\mathbf{k}) P_{jn}(\mathbf{p}) \times P_{ml}(\mathbf{q}) Q(p) Q(q) \} \\ \equiv {} & L_{ijm}(\mathbf{k}, \mathbf{p}, \mathbf{q}). \end{aligned} \tag{8}$$

Thus, $T_{ijm}(\mathbf{k}, \mathbf{p}, \mathbf{q})$ is obtained as the solution to (8). Note that the joint-normal hypothesis [13] also implies (7). However, the joint-normal hypothesis assumes zero triple correlation ($T_{ijm} = 0$), which implies fixed energy spectrum in the inviscid limit. Whereas, the quasi-normal assumption uses (8) to close the triple correlation equation.

It is well known [18,20] that the solution of (8) does not guarantee the positive definiteness of $E(k)$. Therefore, an eddy damping rate $\mu_{kpq} = \mu_k + \mu_p + \mu_q$ is added to the l.h.s of (8) and "markovianization" [18] is applied to get

$$T_{ijm}(\mathbf{k},\mathbf{p},\mathbf{q}) = \theta_{kpq}(t) L_{ijm}(\mathbf{k},\mathbf{p},\mathbf{q}), \tag{9}$$

$$\theta_{kpq}(t) = \int_0^t \exp -[\mu_{kpq} + \nu(k^2+p^2+q^2)](t-\tau)\,\mathrm{d}\tau \approx \frac{1-\exp -[\mu_{kpq}+\nu(k^2+p^2+q^2)]t}{\mu_{kpq}+\nu(k^2+p^2+q^2)}. \tag{10}$$

A few possibilities exist, for the eddy damping rate [18]. We use

$$\mu_k = 0.19 C_k^{3/2}\left[\int_0^k \xi^2 E(\xi)\,\mathrm{d}\xi\right]^{1/2}. \tag{11}$$

Here, C_k is the Kolmogorov constant, which is equal to 1.8 in the present study. Applying (9)–(11), to (5) closes the kinetic energy equation; i.e.,

$$\left(\frac{\partial}{\partial t} + 2\nu k^2\right)E(k) = 8\pi k^2 \int \mathrm{d}^3\mathbf{p}\,\mathrm{d}^3\mathbf{q}\,\delta(\mathbf{p}+\mathbf{q}-\mathbf{k})\theta_{kpq}(t) \times [J_1 Q(p)Q(q) + J_2 Q(k)Q(p) + J_3 Q(k)Q(q)], \tag{12}$$

where the geometrical factors

$$J_1(\mathbf{k},\mathbf{p},\mathbf{q}) = \frac{1}{4}P_{ijm}(\mathbf{k})P_{inl}(\mathbf{k})P_{jn}(\mathbf{p})P_{ml}(\mathbf{q}),$$
$$J_2(\mathbf{k},\mathbf{p},\mathbf{q}) = -\frac{1}{4}P_{ijm}(\mathbf{k})P_{mnl}(\mathbf{q})P_{jn}(\mathbf{p})P_{il}(\mathbf{k}), \tag{13}$$
$$J_3(\mathbf{k},\mathbf{p},\mathbf{q}) = -\frac{1}{4}P_{ijm}(\mathbf{k})P_{jnl}(\mathbf{p})P_{mn}(\mathbf{q})P_{il}(\mathbf{k})$$

are the functions of scalars k, p and q. See Lesieur [18] and Leslie [19] for further simplification of these terms. The three-dimensional double integrations, constrained by $\mathbf{p}+\mathbf{q}=\mathbf{k}$ on the r.h.s of (12) are simplified using [19]

$$\int\int f(k,p,q)\delta(\mathbf{p}+\mathbf{q}-\mathbf{k})\,\mathrm{d}^3\mathbf{p}\,\mathrm{d}^3\mathbf{q} = \int\int_{\Delta_k} \frac{2\pi pq}{k} f(k,p,q)\,\mathrm{d}p\,\mathrm{d}q, \tag{14}$$

where the "triadic domain" Δ_k in (p,q)-plane satisfies $|k-q| \leqslant p \leqslant k+q$. Thus, (12) finally takes the form

$$\left(\frac{\partial}{\partial t} + 2\nu k^2\right)E(k) = \int\int_{\Delta_k} \mathscr{I}(k,p,q)\,\mathrm{d}p\,\mathrm{d}q, \tag{15}$$

$$\mathscr{I}(k,p,q) = \theta_{kpq}\left[J_1 E(p)E(q)\frac{k}{pq} + J_2 E(k)E(p)\frac{q}{kp} + J_3 E(k)E(q)\frac{p}{kq}\right]. \tag{16}$$

Therefore, the evolution equation for the energy spectrum $E(k)$ is a one-dimensional integro-differential equation, which can be easily solved by an accurate numerical method.

2.2. EDQNM-DNS

This section describes the numerical solution of the EDQNM equations, and their validation by comparison to experiment. The solutions are termed EDQNM-DNS, in the sense that all the energetic scales are resolved. For a given number of grid points N, the wavespace is discretized on a logarithmic grid [21]:

$$k(n) = k_0 \cdot 2^{\frac{n-1}{F}}, \quad (n = 1,2,\ldots,N), \tag{17}$$

where k_0 is the smallest wavenumber and the parameter $F(>2)$ determines the resolution. The (p,q)-domain for the integral part of (15) is discretized using the same distribution in each direction. Third order Runge–Kutta, and Crank–Nicolson schemes are adopted for the nonlinear and viscous terms, respectively. An important issue in the numerical integration is that it should guarantee the conservation of total kinetic energy $q^2 = \int E(k)\,\mathrm{d}k$ in the inviscid limit, which requires

$$\int_{k_0}^{k_{\max}} \left\{ \int\int_{\Delta_k} \mathscr{I}(k,p,q)\,\mathrm{d}p\,\mathrm{d}q \right\} \mathrm{d}k = 0. \tag{18}$$

Analytically, EDQNM closure (15) guarantees (18) because of the symmetry. However, this is not always true for the discrete evaluation of $\mathscr{I}(k,p,q)$ and its integration. In this paper, the trapezoidal rule integration is used in direction by direction manner, which discretely satisfies (18). The geometrical factors, J_i's in (13) are functions of the length of wavevectors and, therefore can be uniquely calculated from any choice of $(\mathbf{k},\mathbf{p},\mathbf{q})$ that satisfies $\mathbf{p}+\mathbf{q}=\mathbf{k}$ [19]. For example, $\mathbf{k}=(k,0,0)$, $\mathbf{p}=(p\cos\gamma, p\sin\gamma, 0)$, and $\mathbf{q}=(k-p\cos\gamma, -p\sin\gamma, 0)$ are used in this study, where $\gamma=\cos^{-1}[(p^2+k^2-q^2)/(2pk)]$ is the angle between $\mathbf{p}$ and $\mathbf{k}$. Although conventional EDQNM uses simpler expressions for J_i', [19], we use formulation (13) since it allows the wavevectors to be replaced by "modified wavevectors" [22] to account for numerical discretization error.

Throughout this paper, we use the decaying isotropic turbulence experiments of Comte-Bellot and Corrsin [23] (denoted as CBC hereafter) for validation. These experiments provide energy spectra at three locations. Using the Taylor hypothesis, the spatial locations are converted to time instants of $tU_0/M=42$, 98 and 171, where M(=5.08 cm) and U_0(=10 m/s) are the grid size and the free-stream velocity, respectively. The Taylor micro-scale Reynolds numbers, $Re_\lambda = u_{\mathrm{rms}}\lambda/\nu$, are in the range of 71.6–60.6. The initial conditions in the simulations are a divergence-free random field whose energy spectrum matches that at $tU_0/M=42$. The simulation is performed using $F=8$, $N=65$, and $k_0=1$ which gives the maximum wavenumber $k_c=256$. Here, all wavenumbers are normalized by the reference length scale $L_{\mathrm{ref}}=L_B/2\pi$, where $L_B=11M$ is the side of the computational box. Fig. 1 shows temporal evolution of total kinetic energy and the energy spectra at three locations from EDQNM-DNS and the experimental data. Here, and in what follows, the energy spectrum is non-dimensionalized by L_{ref} and reference velocity scale $U_{\mathrm{ref}}=\sqrt{3/2}u_{\mathrm{rms}}$, which are chosen such that the non-dimensional initial total kinetic energy is 1. As shown in Fig. 1, the EDQNM-DNS and experimental results for total kinetic energy and energy spectra agree very well with each other.

2.3. EDQNM-LES

We extend EDQNM theory to the LES equations where the dynamic Smagorinsky model [24] is used to model the subgrid stresses. The resulting formulation is termed "EDQNM-LES", and is validated against LES performed using the Navier–Stokes equations, termed "NS-LES".

Assume that the LES is performed on a infinite, but discrete space Ω_0 with grid spacing Δ_f. Description of the equation on a discrete space Ω_0 causes nontrivial mathematical problems, including the definition of SGS

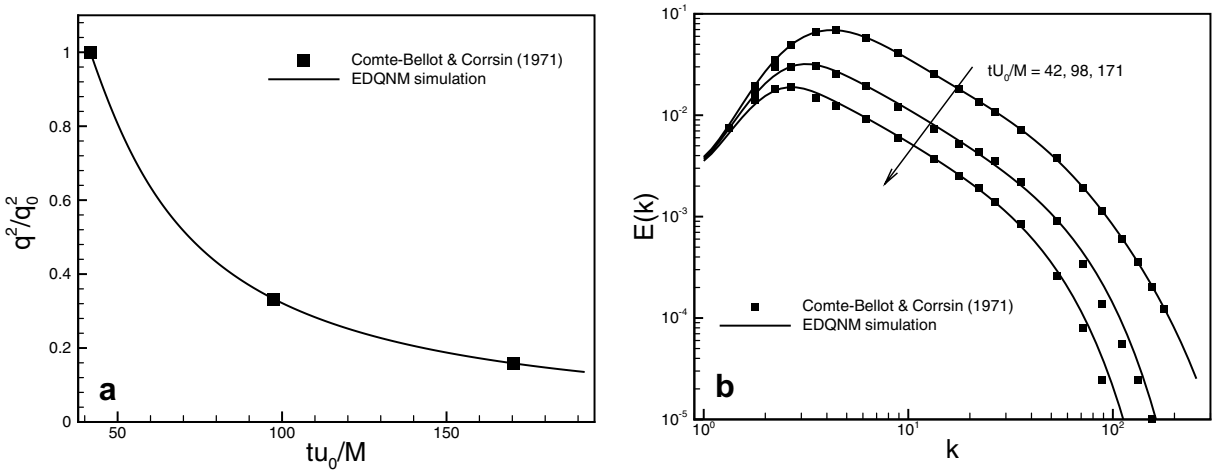

Fig. 1. Time evolution of the total kinetic energy and the energy spectra computed by EDQNM simulation ($k_{\max}=256$) compared with the experimental data of Comte-Bellot and Corrsin [23].

stress [6]. Therefore, consider the equation on the continuous space Ω, and represent the effect of discretization (or finite-dimensional nature) by cutoff filtering with filter width, Δ_f. The LES equations are given by

$$\frac{\partial \widehat{\bar{u}}_i(\mathbf{k})}{\partial t} = -\mathrm{i}P_{imn}(\mathbf{k})H(\mathbf{k})\left[\int_{\square}\int_{\square} \mathrm{d}^3\mathbf{p}\,\mathrm{d}^3\mathbf{q}\,\delta(\mathbf{p}+\mathbf{q}-\mathbf{k})\hat{u}_m(\mathbf{p})\hat{u}_n(\mathbf{q})\right] - \nu k^2 \widehat{\bar{u}}_i(\mathbf{k}) + \widehat{\mathscr{S}}_i(\mathbf{k}), \tag{19}$$

where the domain size $\square = [-k_c, k_c]^3 = [-\pi/\Delta_f, \pi/\Delta_f]^3$, and the filter kernel $H(\mathbf{k}) = 1$ if $\mathbf{k} \in \square$ and $H(\mathbf{k}) = 0$ otherwise. The exact SGS force $\widehat{\mathscr{S}}_i(\mathbf{k}) = -\mathrm{i}P_{imn}(\mathbf{k})H(\mathbf{k})\hat{\tau}_{mn}(\mathbf{k})$ is given by

$$\hat{\tau}_{mn}(\mathbf{k}) = \left(\int\int - \int_{\square}\int_{\square}\right) \mathrm{d}^3\mathbf{p}\,\mathrm{d}^3\mathbf{q}\,\delta(\mathbf{p}+\mathbf{q}-\mathbf{k})\hat{u}_m(\mathbf{p})\hat{u}_n(\mathbf{q}). \tag{20}$$

However, note that use of the exact subgrid model is not only impractical, but also not very meaningful, since the modeled SGS stress τ_{ij}^{M} is used to close (19) in actual simulations. We therefore replace $\mathscr{S}_i$ with the modeled force $\mathscr{S}_i^{\mathrm{M}}$. Including this effect of the modeled SGS stress is very important, since it allows the LES model to interact with numerical error. Section 5 provides more details on this issue. Note that due to modelling error, the solution of this system is no longer the ideal LES solution, $\bar{u}_i$. We will continue to use the symbol $\bar{u}_i$ for notational convenience.

Since LES is essentially a finite-dimensional approximation of the fully resolved solution of the Navier–Stokes equation, the above EDQNM closure can be directly applied to the governing equation for LES. Applying EDQNM closure to (19) using the same procedure as Eqs. (6)–(15), the transport equation for resolved energy spectrum $\overline{E}(k) = 2\pi k^2\langle \widehat{\bar{u}}_i(\mathbf{k})\widehat{\bar{u}}_i(-\mathbf{k})\rangle$ takes the form

$$\begin{aligned}\frac{\partial \overline{E}(k)}{\partial t} &= 8\pi k^2 G(k)\int_{\mathrm{O}}\int_{\mathrm{O}} \mathrm{d}^3\mathbf{p}\,\mathrm{d}^3\mathbf{q}\,\delta(\mathbf{p}+\mathbf{q}-\mathbf{k})\theta_{kpq}[J_1\overline{Q}(p)\overline{Q}(q) + J_2\overline{Q}(k)\overline{Q}(p) + J_3\overline{Q}(k)\overline{Q}(q)] \\ &\quad - 2\nu k^2\overline{E}(k) + T_{\mathrm{SGS}}^{\mathrm{M}}(k), \qquad (21)\\ &= \int\int_{\Delta_k'} \mathrm{d}p\,\mathrm{d}q\,\theta_{kpq}\left[J_1\overline{E}(p)\overline{E}(q)\frac{k}{pq} + J_2\overline{E}(k)\overline{E}(p)\frac{q}{kp} + J_3\overline{E}(k)\overline{E}(q)\frac{p}{kq}\right] - 2\nu k^2\overline{E}(k) + T_{\mathrm{SGS}}^{\mathrm{M}}(k), \qquad (22)\end{aligned}$$

where $T_{\mathrm{SGS}}^{\mathrm{M}}(k) = 4\pi k^2\langle \mathscr{S}_i^{\mathrm{M}}(\mathbf{k})\widehat{\bar{u}}_i(-\mathbf{k})\rangle$ and $\Delta_k' = \Delta_k \cap (p \leqslant k_c, q \leqslant k_c)$. Note that we have replaced the "box" integration domain $\square$ in (19) with the spherical domain $\mathrm{O} = \{\mathbf{k}|\ |\mathbf{k}| \leqslant k_c\}$, and the box cutoff filter $H(\mathbf{k})$ with the spherical filter $G(\mathbf{k})$ ($G(\mathbf{k}) = 1$ if $|\mathbf{k}| \leqslant k_c$ and $G(\mathbf{k}) = 0$ otherwise) accordingly. The truncation of wavevectors near the eight corners of the domain $\square$ is a result of the spherical symmetry of the domain. Note that the true SGS force (20) is used for the derivation of (21) so that the EDQNM closure is not influenced by the SGS model or the numerical error. In what follows, we refer to (22) as reference EDQNM-LES system. The solution of (22) is regarded as the error-free LES solution. Note that this reference system is different from the exact LES equation, and that the modeled SGS transfer $T_{\mathrm{SGS}}^{\mathrm{M}}(k)$ is used instead of the exact term, since we are interested in the effect of the numerical error and SGS model on the computed LES system.

The dynamic Smagorinsky model (DSM) [24] is used for the subgrid stress: $\tau_{ij}^{\mathrm{M}} - \frac{1}{2}\tau_{kk}^{\mathrm{M}}\delta_{ij} = -2\nu_T(\mathbf{x},t)\overline{S}_{ij} = -2C_s\Delta_f^2|\overline{S}|\overline{S}_{ij}$, where $|\overline{S}| = \sqrt{2\overline{S}_{ij}\overline{S}_{ij}}$. It is well known [25,26] that the Smagorinsky model can be approximated by the "plateau" version of the spectral eddy viscosity model [27] in wavespace, which requires the use of the model

$$\tau_{ij}^{\mathrm{M}} - \frac{1}{3}\tau_{kk}^{\mathrm{M}}\delta_{ij} = -2C_s\Delta_f^2\langle\overline{S}\rangle\overline{S}_{ij} = 2\nu_T(t)\overline{S}_{ij} \tag{23}$$

instead of the original DSM. Here, $\langle\overline{S}\rangle$ denotes the ensemble average of $|\overline{S}|$. Let $\mathscr{T}_{ij}^{\mathrm{M}} - \frac{1}{3}\delta_{ij}\mathscr{T}_{kk}^{\mathrm{M}} = -2C_s\Delta_T^2\langle\widetilde{S}\rangle\widetilde{S}_{ij}$ be the subtest scale stress, where $\Delta_T = \alpha\Delta_f$ ($\alpha > 1$) is the size of test filter and $\widetilde{S}_{ij}$ is the test-filtered strain rate tensor. Note that the property $\widetilde{\overline{S}}_{ij} = \widetilde{S}_{ij}$ for the cutoff filter is used. Applying the Germano identity to τ_{ij}^{M} and $\mathscr{T}_{ij}^{\mathrm{M}}$, we get

$$\mathscr{T}_{ij}^{\mathrm{M}a} - \tilde{\tau}_{ij}^{\mathrm{M}a} - L_{ij}^a = \epsilon_{ij}, \tag{24}$$

where the superscript a denotes the traceless tensor, $L_{ij} = \widetilde{\bar{u}_i\bar{u}_j} - \tilde{u}_i\tilde{u}_j$ is the resolved scale stress, and ϵ_{ij} is the error term which should vanish when $\tau_{ij}^{\mathrm{M}} = \tau_{ij}$ and $\mathscr{T}_{ij}^{\mathrm{M}} = \mathscr{T}_{ij}$. The Smagorinsky constant that minimizes $\epsilon_{ij}\epsilon_{ij}$ in the least square sense [28] is

$$C_s\Delta_f^2 = -\frac{\langle L_{ij}\mathscr{R}_{ij}\rangle}{2\langle \mathscr{R}_{kl}\mathscr{R}_{kl}\rangle}, \quad \mathscr{R}_{ij} = \alpha^2\langle\widetilde{S}\rangle\widetilde{S}_{ij} - \widetilde{\langle\overline{S}\rangle\overline{S}_{ij}}. \tag{25}$$

The ensemble averages in (25) are introduced to enhance the stability of the solution. Since $\langle\overline{S}\rangle$ and $\langle\widetilde{S}\rangle$ are constants, (25) can be further simplified to obtain

$$C_s\Delta_f^2 = -\frac{\langle L_{ij}\widetilde{S}_{ij}\rangle}{2\theta\langle\widetilde{S}_{ij}\widetilde{S}_{ij}\rangle}, \tag{26}$$

where $\theta = \alpha^2\langle\overline{S}\rangle - \langle\widetilde{S}\rangle$. We further assume that

$$\langle\overline{S}\rangle = \langle\sqrt{2\overline{S}_{ij}\overline{S}_{ij}}\rangle \approx \sqrt{2\langle\overline{S}_{ij}\overline{S}_{ij}\rangle} = \left(2\int_0^{k_c} k^2\overline{E}(k)\,\mathrm{d}k\right)^{1/2}. \tag{27}$$

Similarly, $\langle\widetilde{S}\rangle$ is approximated as $\langle\widetilde{S}\rangle = \left(2\int_0^{k_T} k^2E(k)\,\mathrm{d}k\right)^{1/2}$. Using this assumption, the eddy viscosity ν_T can be expressed as

$$\nu_T = \frac{\langle L_{ij}\widetilde{S}_{ij}\rangle}{(2-2\alpha^2B)\int_0^{k_T} k^2E(k)\,\mathrm{d}k}, \tag{28}$$

where $B = \left(\int_0^{k_T} k^2E(k)\,\mathrm{d}k / \int_0^{k_c} k^2E(k)\,\mathrm{d}k\right)^{1/2}$. Finally, the expression for $\langle L_{ij}\widetilde{S}_{ij}\rangle = \int_0^{k_T} T^{\mathrm{M}}(k)\,\mathrm{d}k$ should be given. $T^{\mathrm{M}}(k)$ is the transfer spectrum given by

$$T^{\mathrm{M}}(k) = \int_{\mathrm{O}}\int_{\mathrm{O}} M_{ijk}(\mathbf{k})\left\langle \widetilde{U}_i(-\mathbf{k})\left[U_j(\mathbf{p})\widetilde{U_k}(\mathbf{q}) - \widetilde{U}_j(\mathbf{p})\widetilde{U}_k(\mathbf{q})\right]\right\rangle \times \delta^3(\mathbf{p}+\mathbf{q}-\mathbf{k})\,\mathrm{d}^3\mathbf{p}\,\mathrm{d}^3\mathbf{q}. \tag{29}$$

The EDQNM closure can be again used to compute Eq. (29) yielding

$$T^{\mathrm{M}}(k) = \int\int_{\Delta_k''} \mathscr{I}(k,p,q)\,\mathrm{d}p\,\mathrm{d}q. \tag{30}$$

Here, $\mathscr{I}(k,p,q)$ denotes the integrand in Eq. (22). The integration domain Δ_k'' is defined as

$$\Delta_k'' : (p,q \leqslant k_c) \cap (k_T < p \leqslant k_c \quad \text{or} \quad k_T < q \leqslant k_c) \cap (p,q \in \Delta_k), \tag{31}$$

which is illustrated in Fig. 2. Once the eddy viscosity ν_T is obtained, it is straightforward to show that $T^{\mathrm{M}}_{\mathrm{SGS}}(k) = -2\nu_T k^2E(k)$. Thus, the reference EDQNM-LES system (22) is now written as

$$\left[\frac{\partial}{\partial t} + 2(\nu+\nu_T)k^2\right]E(k,t) = \int\int_{\Delta_k'} \mathscr{I}(k,p,q)\,\mathrm{d}p\,\mathrm{d}q. \tag{32}$$

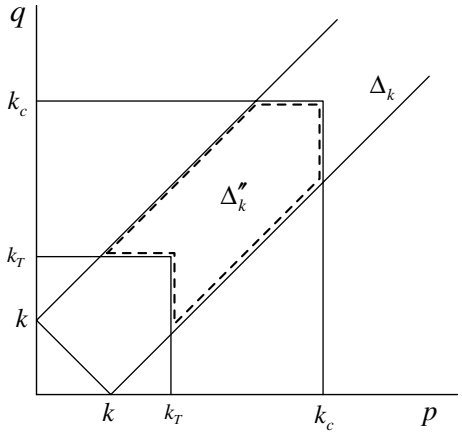

Fig. 2. Domain in the (p,q)-plane Δ_k'' (dashed region) for the evaluation of the dynamic constant in EDQNM-LES with the dynamic Smagorinsky model.

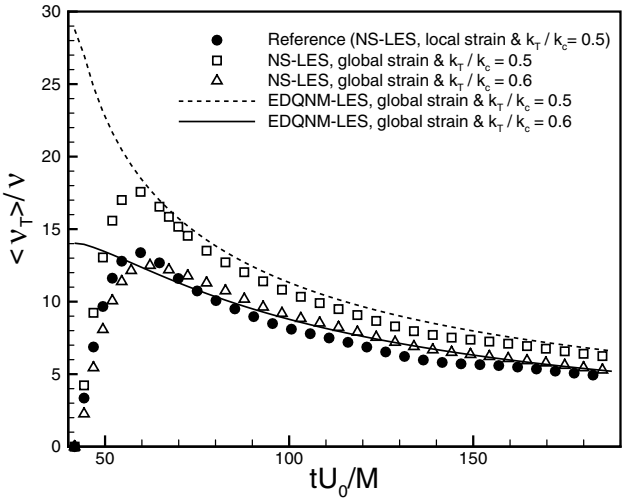

Fig. 3. Effect of the global approximation of $|\overline{S}| = \sqrt{2\overline{S}_{ij}\overline{S}_{ij}}$ and the test filter sizes on SGS dissipation: time evolution of averaged SGS eddy viscosity.

The only adjustable parameter in DSM is $\alpha = \Delta_T/\Delta_f = k_c/k_T$. The computation with the typical choice of $\alpha = 2$ ($k_T = 0.5k_c$) results in $C_s \approx 0.2$, which is about 30% higher than $C_s \approx 0.15$, a common value obtained for isotropic turbulence.

Recall the use of global strain rate $\langle\overline{S}\rangle$ instead of the local value. The impact of this assumption on SGS dissipation was tested by performing LES of the Navier–Stokes equations (denoted as NS-LES hereafter) using DSM with the global strain rate. The NS-LES uses a dealiased pseudo-spectral method, and semi-implicit time discretization at 32^3 resolution. See Ref. [12] for more details on the numerical method. Results from the NS-LES are plotted in Fig. 3, which shows the time evolution of volume-averaged eddy viscosity $\langle\nu_T\rangle$ normalized by the molecular viscosity. As shown in figure, NS-LES overpredicts the SGS dissipation when the global strain rate is used, for $\alpha = 2$. Also, the evolution of SGS eddy viscosity from NS-LES in this case is in good agreement with that from EDQNM-LES. The discrepancy observed in the initial stages is due to

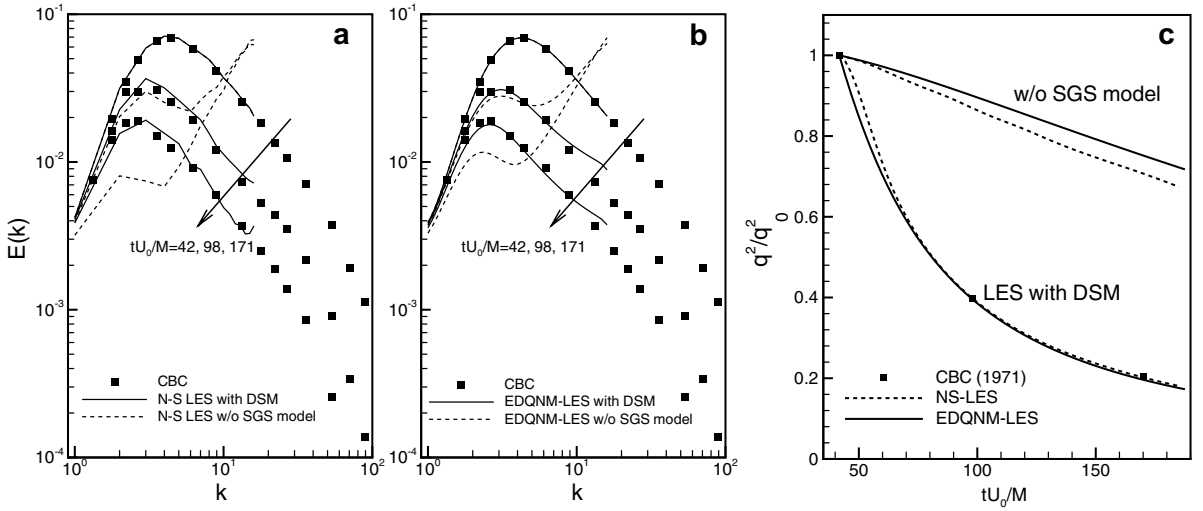

Fig. 4. NS-LES and EDQNM-LES with and without SGS model: three-dimensional energy spectra for (a) NS-LES and (b) EDQNM-LES; (c) time evolution of resolved total kinetic energy.

the random-phase initialization of NS-LES that gives initial $C_s \approx 0$. It is also clear that NS-LES with global strain rate agrees well (in terms of SGS dissipation) with the reference solution using local strain rate, when $\alpha = 5/3$, ($k_T/k_c = 0.6$). This result again is in good agreement with that from EDQNM-LES. Thus, in what follows, $\alpha = 5/3$ is adopted for EDQNM-LES and results are compared with NS-LES results with $\Delta_T = 2\Delta_f$ as the "compensation" for the use of global strain rate.

The results from two reference simulations (19) and (22) with DSM mentioned above are compared in Fig. 4, together with results without SGS models. Here and in what follows, all EDQNM-LES simulations are performed with $N = 33$ ($k_0 = 1, F = 8$). This corresponds to the cutoff wavenumber $k_c = 16$ at which NS-LES is conducted. As shown in Fig. 4, EDQNM-LES agrees well with NS-LES for both the energy spectra and resolved kinetic energy, with and without SGS model. Note that resolved kinetic energy is compared with filtered experimental data at Δ_f. When the SGS model is turned off, a large pile-up of energy is observed. This demonstrates that the role of molecular viscosity is small and, thus the contribution of SGS model is significant in stabilizing the solution. It is also remarkable to see a good agreement between results from NS-LES and EDQNM-LES, without SGS model. This shows the reliability of EDQNM closure even in situations far removed from well-resolved isotropic turbulence.

3. Numerical errors

Finite-difference simulations involve two distinct sources of numerical error: finite-differencing error and aliasing error. In this section, we incorporate these sources of numerical errors individually in the reference EDQNM-LES system, and perform LES of CBC-isotropic turbulence. These results are validated against those from corresponding NS-LES.

3.1. Finite-differencing error due to the nonlinear term

A staggered second order-finite difference scheme (denoted as SCD2) is considered, which takes the form

$$N_i^s = \frac{\delta_1}{\delta_1 x_j}(\overline{v_i}^{x_j}\overline{v_j}^{x_i}), \tag{33}$$

where the notation of Morinishi et al. [29] is used for the difference operator $\delta_1(\ )/\delta_1 x_j$ and the averaging operator $\overline{(\ )}^{x_i}$. Note that the summation convention is not applied to the averaging operators. Applying SCD2 to (19), we get

$$\frac{\partial \hat{v}(\mathbf{k},t)}{\partial t} = -\mathrm{i}P_{imn}(\mathbf{k}')H(\mathbf{k})\left[\int_{\square}\int_{\square} \mathrm{d}^3\mathbf{p}\,\mathrm{d}^3\mathbf{q}\,\delta(\mathbf{p}+\mathbf{q}-\mathbf{k})\hat{v}_m(\mathbf{p},t)k_a^1(\mathbf{p})\hat{v}_n(\mathbf{q},t)k_a^2(\mathbf{q})\right] - \nu k^2\hat{v}_i(\mathbf{k},t) - \mathrm{i}P_{imn}(\mathbf{k})\hat{\tau}^{\mathrm{M}}_{mn}(\mathbf{k},t), \tag{34}$$

where $\mathbf{k}'$ is the modified wavevector [22], which results from the finite-difference approximation of the first derivative, and k_a^1 and k_a^2 denote modified wavenumbers for the averaging operators in SCD2. Note that numerical error due to time integration is neglected. For SCD2, the modified wavenumber and averaging factors are given as

$$k'_m\Delta_g = 2\sin(k_m\Delta_g/2), k_a^1(\mathbf{p}) = \cos(p_n\Delta_g/2), \quad k_a^2(\mathbf{q}) = \cos(q_m\Delta_g/2). \tag{35}$$

Here, Δ_g is the grid size that is not necessarily equal to the filter size Δ_f. However, we assume $\Delta_g = \Delta_f$ throughout this paper. The fact that the solution of (34) is denoted by v_i rather than $\bar{u}_i$ reflects the deviation of the solution from the reference value due to the finite-differencing error. This distinction is important since the comparison between $\bar{u}_i$ and v_i reveals the numerical error as will be shown later.

Then, the corresponding nonlinear transport term of reference EDQNM-LES is

$$T_r(k) = 4\pi k^2 M_{ijm}(\mathbf{k}')G(\mathbf{k})\int_{\mathrm{O}}\int_{\mathrm{O}} T'_{ijm}\delta(\mathbf{p}+\mathbf{q}-\mathbf{k})\,\mathrm{d}^3\mathbf{p}\,\mathrm{d}^3\mathbf{q}, \tag{36}$$

$$T'_{ijm}(\mathbf{k},\mathbf{p},\mathbf{q}) = \langle \hat{v}_i(-\mathbf{k})\hat{v}_j(\mathbf{p})k_a^1(p_m)\hat{v}_m(\mathbf{q})k_a^2(q_j)\rangle. \tag{37}$$

Because of the directional dependence of the averaging factors, it is not straightforward to apply the quasi-normal hypothesis to (36). In order to circumvent this difficulty, we introduce the following assumption:

$$T'_{ijm}(\mathbf{k},\mathbf{p},\mathbf{q}) \approx \langle k_a^1(p_m)k_a^2(q_j)\rangle\langle \hat{v}_i(-\mathbf{k})\hat{v}_j(\mathbf{p})\hat{v}_m(\mathbf{q})\rangle \tag{38}$$

$$\approx A(p)A(q)T_{ijm}(\mathbf{k},\mathbf{p},\mathbf{q}), \tag{39}$$

where A is the isotropic averaging factor

$$A(p) = \{k_a(p_m)^1\}_p = \frac{1}{4\pi}\int_0^{2\pi}\int_0^{\pi} \cos[(p\cos\theta)\Delta_g/2]\sin\theta\,\mathrm{d}\theta\,\mathrm{d}\phi. \tag{40}$$

Here, the first component of $\mathbf{p}$, or $p_1 = p\cos\theta$ is used to evaluate $A(p)$, but the same result is obtained with $p_2 = p\sin\theta\cos\phi$ or $p_3 = p\sin\theta\sin\phi$ due to the isotropy. Thus, the directional sensitivity of the averaging factor is removed. Using (39), it is straightforward to obtain the following modification of the reference system:

$$\left[\frac{\partial}{\partial t} + 2(\nu + \nu_T^{\mathrm{c}})k^2\right]E^{\mathrm{c}}(k,t) = \int\int_{\Delta'_k} A(p)A(q)\mathscr{I}^{\mathrm{c}}(k,k',p,q)\,\mathrm{d}p\,\mathrm{d}q, \tag{41}$$

$$\mathscr{I}^{\mathrm{c}}(k,k',p,q) = \theta_{kpq}\left[J'_1E^{\mathrm{c}}(p)E^{\mathrm{c}}(q)\frac{k}{pq} + J'_2E^{\mathrm{c}}(k)E^{\mathrm{c}}(p)\frac{q}{kp} + J'_3E^{\mathrm{c}}(k)E^{\mathrm{c}}(q)\frac{p}{kq}\right], \tag{42}$$

where

$$J'_1(\mathbf{k},\mathbf{k}',\mathbf{p},\mathbf{q}) = \frac{1}{4}P_{ijm}(\mathbf{k}')P_{inl}(\mathbf{k})P_{jn}(\mathbf{p})P_{ml}(\mathbf{q}) \tag{43}$$

and $J'_2(\mathbf{k},\mathbf{k}',\mathbf{p},\mathbf{q})$ and $J'_3(\mathbf{k},\mathbf{k}',\mathbf{p},\mathbf{q})$ are defined in a similar manner. The reason that the modified wavevectors are considered only for the first term $P_{ijm}(\mathbf{k}')$, is that other terms are invoked during the closure of T_{ijm}. $E^{\mathrm{c}}(k)$ denotes the spectrum of the solution that is contaminated by finite-differencing errors in the convection term. The expression ν_T^{c} indicates that the numerical error also influences the computation of eddy viscosity (see Section 5).

$E^{\mathrm{c}}(k)$ computed from (41) and (42) is shown in Fig. 5, together with the spectrum from the corresponding NS-LES system, (34) and (35). As shown in Fig. 5, the agreement between two results are good, in that $E^{\mathrm{c}}(k)$ is larger than $E(k)$ in the intermediate wavenumbers and smaller near the cutoff. Consequently, total kinetic energy is overpredicted by up to 20% in the presence of the finite-differencing error (Fig. 5(c)).

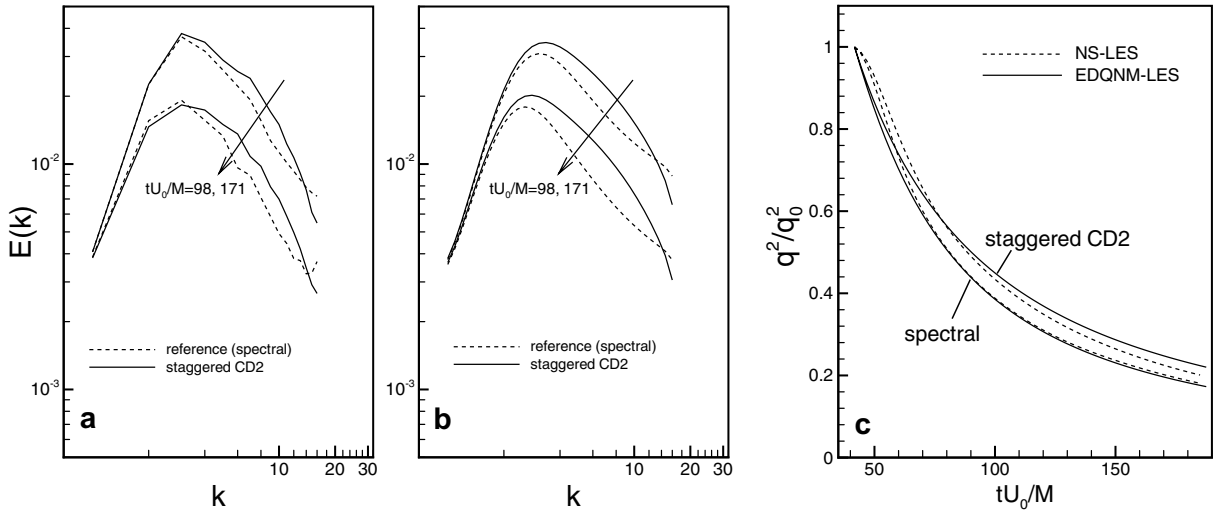

Fig. 5. NS-LES and EDQNM-LES with second-order central difference scheme in a staggered grid: three-dimensional energy spectra for (a) NS-LES and (b) EDQNM-LES; (c) time evolution of resolved total kinetic energy.

Note that the conservative second-order scheme on a collocated mesh $N_i^c = \frac{\delta_1}{\delta_1 x_j}(\overline{v_i}^{x_j}\overline{v_j}^{x_j})$ is approximated by the same form as (39), due to the symmetry of the averaging factor. We conducted NS-LES with N_i^c to obtain essentially the same result with that from SCD2 reported in this section (not shown here). Note also that the skew-symmetric form of the nonlinear term on a regular mesh, is equivalent to N_i^c for second order scheme, as shown by Ducros et al. [30]. However, in actual simulations in physical space, kinetic energy is not exactly conserved for the collocated scheme N_i^c due to the conservation error from pressure gradient term [16].

3.2. Finite-differencing error due to viscous and SGS term

Next, the finite-differencing error due to the viscous and SGS terms is considered. When the finite difference scheme is applied to the second derivative of (32), it would take the form

$$\left[\frac{\partial}{\partial t} + 2(\nu + \nu_T^v)k_{3D}''^2(k)\right]E^v(k,t) = \int\int_{\Delta_k'} \mathscr{I}^v(k,p,q)\,\mathrm{d}p\,\mathrm{d}q, \tag{44}$$

where $E^v(k)$ denotes the energy spectrum of the solution that is contaminated by finite-differencing errors in the viscous and SGS terms. $k_{3D}''^2$ is the three-dimensional, or the spherical shell-averaged modified wavenumber defined by

$$k_{3D}''^2(k) = \frac{1}{4\pi}\int_0^{2\pi}\int_0^{\pi}[k''^2(k_1) + k''^2(k_2) + k''^2(k_3)]\sin\theta\,\mathrm{d}\theta\,\mathrm{d}\phi, \tag{45}$$

where k''^2 is the one-dimensional modified wavenumber for second derivative. In this study, we consider the following two schemes for an arbitrary function ϕ defined on uniform grid:

$$\frac{\delta^2\phi}{\delta x^2} = \frac{\phi_{j+1} - 2\phi_j + \phi_{j-1}}{\Delta_g^2} \rightarrow k''^2\Delta_g^2 = 2[1 - \cos(k\Delta_g)], \tag{46}$$

$$\frac{\delta}{\delta x}\left(\frac{\delta\phi}{\delta x}\right) = \frac{\phi_{j+2} - 2\phi_j + \phi_{j-2}}{4\Delta_g^2} \rightarrow k''^2\Delta_g^2 = \sin^2(k\Delta_g), \tag{47}$$

where subscripts $j, j+1, \ldots$ denote discrete grid indices. Eq. (46) corresponds to the conventional three-point stencil, second order central difference (denoted as 3pt-stencil CD2), and (47) is obtained by the double applications of the first derivative, that results in a five-point stencil scheme (5pt-stencil CD2) in physical space. Although this scheme is rarely used in incompressible simulations, compressible flow simulations often use schemes similar to (47) due to the complexity of the viscous term (see, e.g. Ref. [31]). In the context of LES, the 5pt-stencil CD2 may appear even in the incompressible simulation, if one implements the SGS model in the form $-\frac{\partial}{\partial x_j}\tau_{ij}$. In that case, if $\tau_{ij}^a = -\nu_T(\partial v_i/x_j + \partial v_j/x_i)$ and its derivatives are evaluated at the same point using the second-order central difference, the resulting algorithm corresponds to the 5pt-stencil CD2.

Three-dimensional modified wavenumbers for 3pt- and 5pt-stencil CD2 given by (45) are shown in Fig. 6. Note the superiority of the compact stencil scheme. $E^v(k)$ and total kinetic energy predicted from (44) with 3pt- and 5pt-stencil CD2 are shown in Fig. 7, together with comparable results from NS-LES. The agreement between results from EDQNM-LES and NS-LES is excellent for the spectra and the evolution of resolved kinetic energy. It is shown that results from 5pt-stencil CD2 are unacceptably erroneous, as expected from the modified wavenumber behavior. The error causes reduced dissipation at high wavenumbers, which results in the pile-up of the energy at high wavenumbers, and slow decay of resolved kinetic energy (Fig. 7(c)). In this problem, this pile-up is mostly caused by the lack of SGS dissipation, which is about 10 times larger than viscous dissipation as shown in Fig. 3.

3.3. Aliasing error

Aliasing error arises due to the point-wise multiplication in physical space to compute the nonlinear term [6,7]. Including the aliasing error in (19), we get

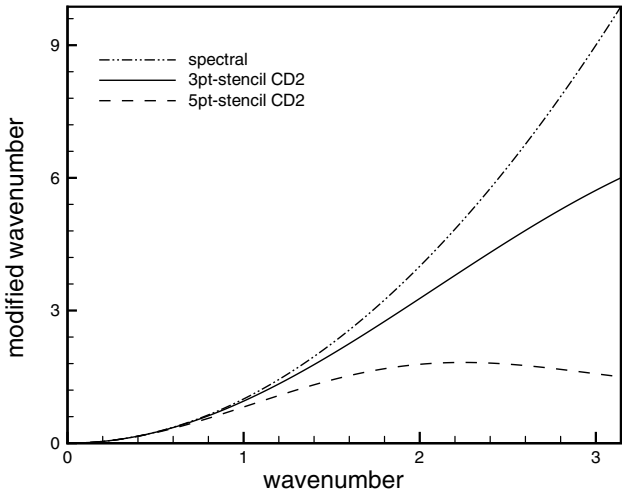

Fig. 6. Three-dimensional (spherical) modified wavenumbers for second derivative.

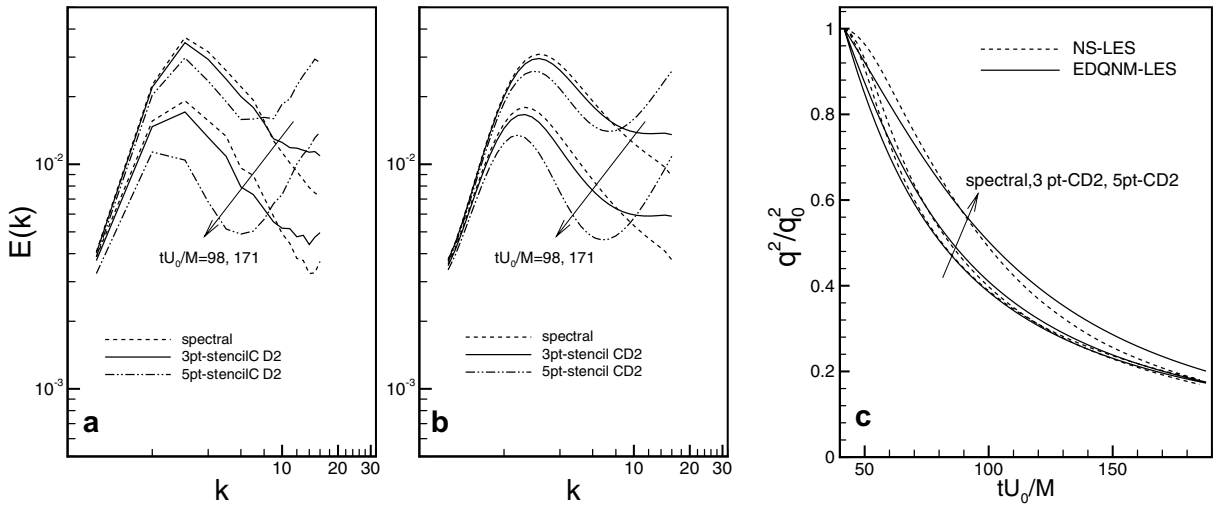

Fig. 7. NS-LES and EDQNM-LES with three-point and five-point stencil second-order central difference schemes for second derivative: three-dimensional energy spectra for (a) NS-LES and (b) EDQNM-LES; (c) time evolution of resolved total kinetic energy.

$$\frac{\partial \hat{v}_i(\mathbf{k},t)}{\partial t} = -\mathrm{i}P_{imn}(\mathbf{k})H(\mathbf{k}')\left[\sum_{\mathbf{a}\in\Lambda}\int_{\square}\int_{\square}\mathrm{d}^3\mathbf{p}\,\mathrm{d}^3\mathbf{q}\,\delta(\mathbf{p}+\mathbf{q}-\mathbf{k}-\mathbf{a})\hat{v}_m(\mathbf{p},t)k_a^1(\mathbf{p})\hat{v}_n(\mathbf{q},t)k_a^2(\mathbf{q})\right] - \nu k^2\hat{v}_i(\mathbf{k},t) + \widehat{\mathscr{S}}_i^{\mathrm{M}}(\mathbf{k}), \tag{48}$$

where Λ is the set of wavevectors of the form $(2pk_c, 2qk_c, 2rk_c)$, where p, q, and r can independently take on values of 0 or ± 1. All modes except for $(0,0,0)$ represents aliasing errors. To highlight aliasing error, finite-differencing error is excluded so that $\mathbf{k}' = k$ and $k_a^1 = k_a^2 = 1$ are assumed during the derivation of EDQNM expression for the aliasing error. Later in this section, we will again consider the modified wavenumbers and averaging factors for the aliasing error of SCD2.

Multiplying by $\hat{v}_i(-\mathbf{k})$ and taking the ensemble average of (48) yields the following expression for the aliasing error:

$$T_{\mathrm{alias}}(\mathbf{k}) = 4\pi k^2 M_{ijm}(\mathbf{k})G(\mathbf{k})\sum_{\mathbf{a}\in\Lambda_0}\int_{\mathrm{O}}\int_{\mathrm{O}}\mathrm{d}^3\mathbf{p}\,\mathrm{d}^3\mathbf{q}\,\delta(\mathbf{p}+\mathbf{q}-\mathbf{k}-\mathbf{a})\times\langle\hat{v}_i(-\mathbf{k})\hat{v}_j(\mathbf{p})\hat{v}_m(\mathbf{q})\rangle, \tag{49}$$

where $\Lambda_0 = \Lambda - (0,0,0)$ denotes the pure aliasing modes, and here again spherical symmetry is assumed. Since the transport equation of $\langle \hat{v}_i(-\mathbf{k})\hat{v}_j(\mathbf{p})\hat{v}_m(\mathbf{q})\rangle$ should have the same form as (8) except that $\mathbf{p}+\mathbf{q} = \mathbf{k}+\mathbf{a}$, it is easy to show that (49) is modeled by EDQNM theory as

$$T_{\text{alias}}(\mathbf{k}) = \sum_{\mathbf{a}\in\Lambda_0} \int_{\mathrm{O}} \int_{\mathrm{O}} \mathrm{d}^3\mathbf{p}\,\mathrm{d}^3\mathbf{q}\,\delta(\mathbf{p}+\mathbf{q}-\mathbf{k}-\mathbf{a}) \frac{k}{2\pi pq}\left[J_1 E^a(p)E^a(q)\frac{k}{pq} + J_2 E^a(k)E^a(p)\frac{q}{kp} + J_3 E^a(k)E^a(q)\frac{p}{kq}\right] \tag{50}$$

$$= \sum_{\mathbf{a}\in\Lambda_0} \int\int_{\Delta'_{|\mathbf{k}+\mathbf{a}|}} \frac{k}{|\mathbf{k}+\mathbf{a}|}\mathscr{I}^a(k,p,q)\,\mathrm{d}p\,\mathrm{d}q. \tag{51}$$

Here, E^a denotes the energy spectrum contaminated by the aliasing error, and $\Delta'_{|\mathbf{k}+\mathbf{a}|}$ denotes the same form of triadic domain as Δ'_k, except that k is replace by $|\mathbf{k}+\mathbf{a}|$. In deriving (51), the formulation [19]

$$\int_{\mathrm{O}} \int_{\mathrm{O}} f(k,p,q)\delta(\mathbf{p}+\mathbf{q}-\mathbf{k}-\mathbf{a})\,\mathrm{d}^3\mathbf{p}\,\mathrm{d}^3\mathbf{q} = \int\int_{\Delta'_{|\mathbf{k}+\mathbf{a}|}} \frac{2\pi pq}{|\mathbf{k}+\mathbf{a}|} f\,\mathrm{d}p\,\mathrm{d}q \tag{52}$$

is invoked, which directly comes from (14). Since (51) depends on the vector $\mathbf{k}$, the aliasing error $T^s_{\text{alias}}(k)$ to be added to (32) requires an additional spherical shell average to yield

$$T^s_{\text{alias}}(k) = \frac{1}{4\pi}\sum_{\mathbf{a}\in\Lambda_0}\int_0^{2\pi}\int_0^{\pi}\left[\int\int_{\Delta_{|\mathbf{k}+\mathbf{a}|}} \frac{k}{|\mathbf{k}+\mathbf{a}|}\mathscr{I}^a(k,p,q)\,\mathrm{d}p\,\mathrm{d}q\right]\sin\theta\,\mathrm{d}\theta\,\mathrm{d}\phi \tag{53}$$

$$= 6T^{1\mathrm{D}}_{\text{alias}}(k) + 12T^{2\mathrm{D}}_{\text{alias}}(k) + 8T^{3\mathrm{D}}_{\text{alias}}(k), \tag{54}$$

where $T^{1\mathrm{D}}_{\text{alias}}$ is the one-dimensional aliasing mode from any of six vectors $\mathbf{a} = (\pm 2k_c,0,0)$, $(0,\pm 2k_c,0)$, or $(0,0,\pm 2k_c)$. Two and three-dimensional modes $T^{2\mathrm{D}}_{\text{alias}}$ and $T^{3\mathrm{D}}_{\text{alias}}$ are defined similarly [6] and therefore computation of three modes is required instead of $3^3 - 1 = 26$ modes. However, the computational overhead to compute (53) is very high and thus EDQNM-LES with the aliasing error requires as much computational time as NS-LES.

In order to retain the simplicity of EDQNM-LES, an approximate evaluation of the aliasing term is performed. We assume that the aliasing error for a given k occurs only through a representative value of $|\mathbf{k}+\mathbf{a}| \equiv K$ defined by

$$K(k,\mathbf{a}) = \frac{1}{A_{\text{alias}}(k)}\int_0^{2\pi}\int_0^{\pi} H(2k_c - |\mathbf{k}+\mathbf{a}|)|\mathbf{k}+\mathbf{a}|k^2\sin\theta\,\mathrm{d}\theta\,\mathrm{d}\phi, \tag{55}$$

where H is the heaviside function and $A_{\text{alias}}(k)$ is the area of the part of the spherical shell that corresponds to the aliasing mode, or $A_{\text{alias}}(k) = \int_0^{2\pi}\int_0^{\pi} H(2k_c - |\mathbf{k}+\mathbf{a}|)k^2\sin\theta\,\mathrm{d}\theta\,\mathrm{d}\phi$. Thus, (55) is the conditional shell average of $|\mathbf{k}+\mathbf{a}|$ under the condition that $|\mathbf{k}+\mathbf{a}|$ belongs to the aliasing mode. Once K is given, the aliasing error is approximated by

$$T^s_{\text{alias}}(k) \approx \left(\frac{A_{\text{alias}}(k)}{4\pi k^2}\right)\sum_{\mathbf{a}\in\Lambda_0}\int\int_{\Delta'_K}\frac{k}{K(k,\mathbf{a})}\mathscr{I}^a(k,p,q)\,\mathrm{d}p\,\mathrm{d}q. \tag{56}$$

The "exact" aliasing term within the EDQNM context (53), and the approximation (56) are compared in Fig. 8 for the spectral method and SCD2 for the initial field of CBC-isotropic turbulence at $tU_0/M = 42$. The aliasing error of SCD2 is derived from (48) and (36)–(40). It is shown that the approximated aliasing error shows similar behavior in the wavespace, and that the agreement is reasonable except for high wavenumber regions near the cutoff. As expected, the aliasing error from SCD2 is smaller than that from the spectral method.

Inserting the aliasing error in (32), we get the EDQNM-LES system for an aliased spectral method:

$$\left[\frac{\partial}{\partial t} + 2(\nu+\nu^a_T)k^2\right]E^a(k,t) = \int\int_{\Delta'_k}\mathscr{I}^a(k,p,q)\,\mathrm{d}p\,\mathrm{d}q + T^s_{\text{alias}}(k). \tag{57}$$

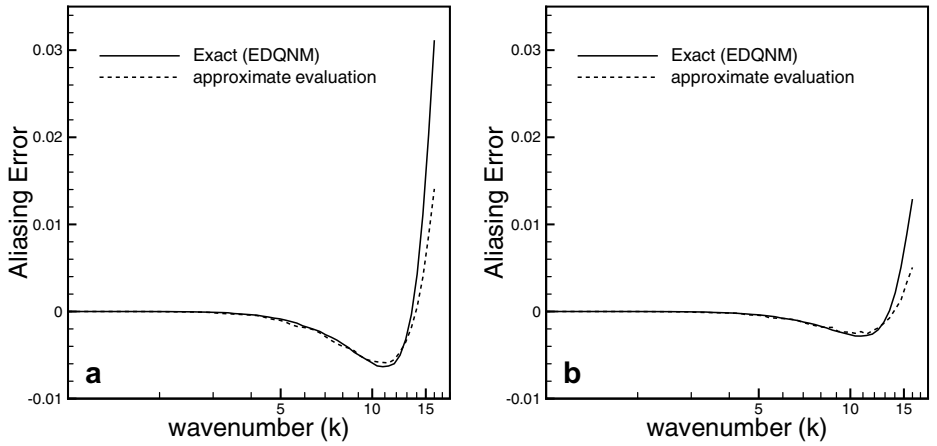

Fig. 8. The transfer functions of aliasing error for the initial field of CBC-isotropic turbulence ($tU_0/M = 42$): (a) spectral method; (b) staggered second order central difference.

$E^a(k)$, the solution of (57), is shown in Fig. 9 together with comparable results from NS-LES. The most noticeable aspect of the aliasing error in Fig. 9, is that the error is small. The aliasing error is shown to contaminate only very high wavenumber region so that total kinetic energy evolution is nearly unchanged for both NS-LES and EDQNM-LES. It is also shown that the approximate aliasing error is acceptable, to represent the effect of aliasing error; i.e. the approximation is satisfactory, except at very high wavenumber regions, and that the aliasing error itself does not contribute significantly to the solution.

This result may contradict previous studies (see, e.g. [7]) that emphasized the significance of the aliasing error. One possible reason is the use of the spherical cutoff filter which removes energy at resolved wavenumbers in the range $k_c < k < \sqrt{3}k_c$. Thus, a part of the aliasing error is removed by this filter. Actually the aliasing error defined in this manner corresponds to the "lower bound" of true aliasing error defined in domain □ [6]. Another possible explanation is accumulation of the "conservation error". It is well known that aliased Fourier spectral methods do not conserve the total kinetic energy when the nonlinear term is written in divergence form [7]. Thus, in this case, the conservation error is the main characteristic of the aliasing error, whose cumulative effect can be revealed only through a long time integration. However, EDQNM-LES even with the

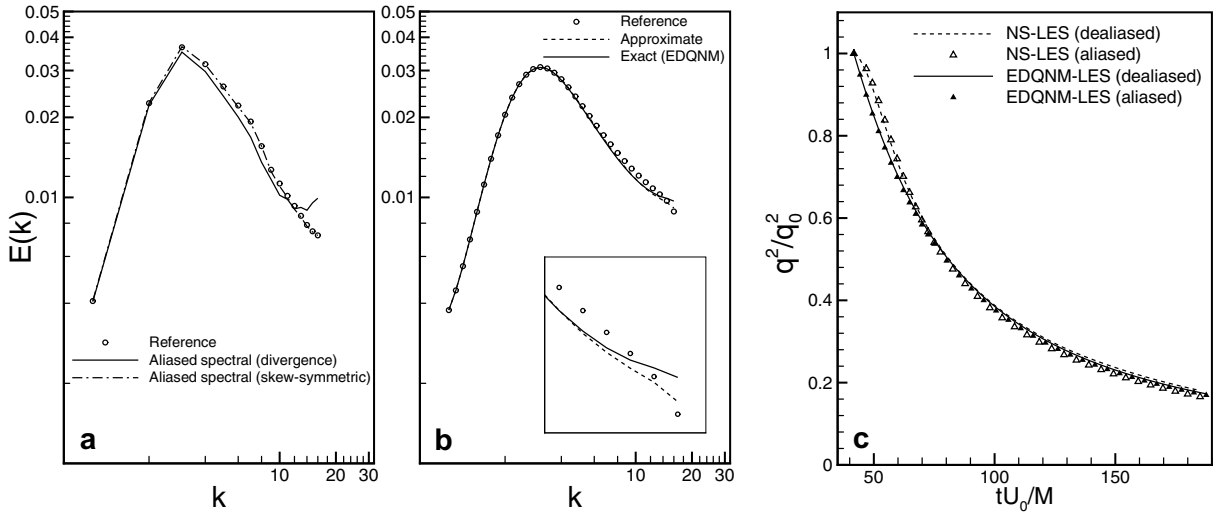

Fig. 9. NS-LES and EDQNM-LES with aliased spectral method: three-dimensional energy spectra at $tU_0/M = 98$ for (a) NS-LES and (b) EDQNM-LES; (c) time evolution of resolved total kinetic energy.

aliased spectral method (53) conserves the total kinetic energy so that this aspect is not correctly modeled with EDQNM closure (see Appendix A for more discussion on the conservation issue.)

Since the divergence form of the spectral method violates "local" conservation as well as global conservation [7], it is expected that the error appears as a source term at each control volume (= grid) where the local conservation is defined. Therefore, the conservation error should grow from very high-wavenumber regions near the cutoff. This explains the difference between the energy spectra predicted by NS-LES and EDQNM-LES in Fig. 9(a) and (b).

In order to support this argument, the energy spectrum from NS-LES with aliased spectral method with skew-symmetric nonlinear term is shown in Fig. 9(a), which is indistinguishable from the reference solution with dealiased spectral method. It is well known that the skew-symmetric form conserves the kinetic energy, even in the presence of the aliasing error [7]. Therefore, it appears that the aliasing error matters only when it causes the violation of the kinetic energy conservation. Otherwise, its effect should be small. In this sense, the failure of EDQNM-LES in predicting conservation error for the spectral method will not cause any problem in the results that will be given in Section 4 for SCD2, since EDQNM-LES shows good conservation property for SCD2 with and without aliasing error (see Appendix A).

4. Modeling numerical error in second-order LES code

4.1. EDQNM model

Combining all the elements introduced in Section 3, we construct a complete EDQNM model for an actual LES code with second-order accurate finite-difference scheme. The model takes the form:

$$\left[\frac{\partial}{\partial t}+2(\nu+\nu_T^{\mathrm{CD2}})k_{3\mathrm{D}}''^2\right]E^{\mathrm{CD2}}(k)=\int\int_{\Delta_k'}A(p)A(q)\mathscr{I}^{\mathrm{CD2}}\,\mathrm{d}p\,\mathrm{d}q + \left(\frac{A_{\mathrm{alias}}(k)}{4\pi k^2}\right)\left[\sum_{\mathbf{a}\in\Lambda_0}\int\int_{\Delta_K'}\frac{k}{K(k,\mathbf{a})}A(p)A(q)\mathscr{I}^{\mathrm{CD2}}\,\mathrm{d}p\,\mathrm{d}q\right], \tag{58}$$

where the energy spectrum from this system is denoted by $E^{\mathrm{CD2}}(k)$. SCD2 is adopted for the nonlinear term and the aliasing error, and 3pt-stencil second order difference is adopted for the viscous term.

Fig. 10 shows the energy spectra and kinetic energy evolution computed by (58) and those from corresponding NS-LES. Here again, the agreement between EDQNM-LES and NS-LES is good in that the spectra

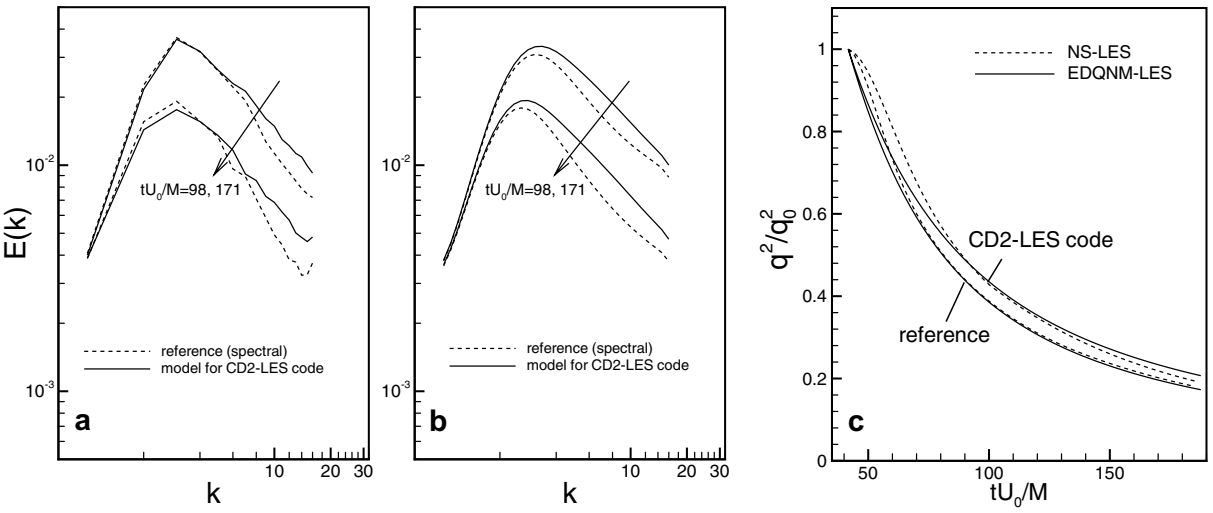

Fig. 10. NS-LES and EDQNM-LES as the model for the LES code with second-order central difference scheme: three-dimensional energy spectra for (a) NS-LES and (b) EDQNM-LES; (c) time evolution of resolved total kinetic energy.

from both simulation show the overprediction at intermediate and high wavenumber regions. From the comparison among Figs. 5, 7 and 10, it appears that the overprediction of energy at intermediate wavenumbers is mainly due to the finite differencing error associated with the convection term, and the overprediction at high wavenumber is due to finite differencing error of viscous term. As shown in Fig. 10, numerical error leads to approximately 10% overprediction of total kinetic energy. However, a more important issue is how this error affects the performance of the SGS model, and if the SGS model is masked by this error.

4.2. Relative magnitudes of error

A dynamic error analysis of LES with a second-order central difference scheme is performed. Dynamic error analysis implies that the effect of numerical errors and SGS terms are traced by their contribution to the solution.

In Section 3, the reference system uses a dealiased spectral method and individual components of numerical errors and SGS model were individually introduced. This approach is effective as a means to validate the EDQNM-LES system, and the impact of numerical error. In order to evaluate the numerical error for the second-order central difference scheme, $E^{\mathrm{CD2}}(k)$, the solution of (58) is used as the reference solution in this section. Then, the contribution of SGS model, finite-differencing error, and aliasing error are evaluated by "turning off" each element from the reference system of (58). For example, the contribution of SGS term σ^{SGS} is defined by

$$\sigma^{\mathrm{SGS}}(t) = \frac{\int_0^{k_c} |E^{\mathrm{CD2}}(k,t) - E^{\mathrm{CD2}}_{\mathrm{SGS}-}(k,t)|\,\mathrm{d}k}{\int_0^{k_c} E^{\mathrm{CD2}}(k)\,\mathrm{d}k}, \tag{59}$$

where $E^{\mathrm{CD2}}_{\mathrm{SGS}-}(k)$ denotes the solution of (58) with $\nu_T = 0$. The contribution of numerical errors are defined in a similar way. For example, the contribution of the aliasing error is defined by replacing $E^{\mathrm{CD2}}_{\mathrm{SGS}-}(k)$ in (59) with the spectra from dealiased finite differencing scheme. Resolved kinetic energy of the reference solution is used to normalize each contribution.

Fig. 11 shows the contribution of the SGS model and numerical errors for two cutoff wavenumbers $k_c = 16$ and $k_c = 32$ for CBC-isotropic turbulence. It is clear that the SGS contribution overwhelms all numerical errors, whose magnitude is comparable or larger than resolved kinetic energy. On the other hand, the magnitude of total error is less than 10% of resolved kinetic energy for both cutoff wavenumbers, which is consistent with total kinetic energy evolution in Fig. 10(c). The contribution of total numerical error is evaluated from (59) by replacing $E^{\mathrm{CD2}}_{\mathrm{SGS}-}(k)$ with $\overline{E}(k)$, or reference solution. Note that total numerical error is even smaller than the contribution of convection term alone. Comparison of $E^{c}(k)$ (Fig. 5) and $E^{\mathrm{CD2}}(k)$ (Fig. 10) suggests that the viscous term error reduces the overprediction of energy at intermediate wavenumbers, that is caused by the

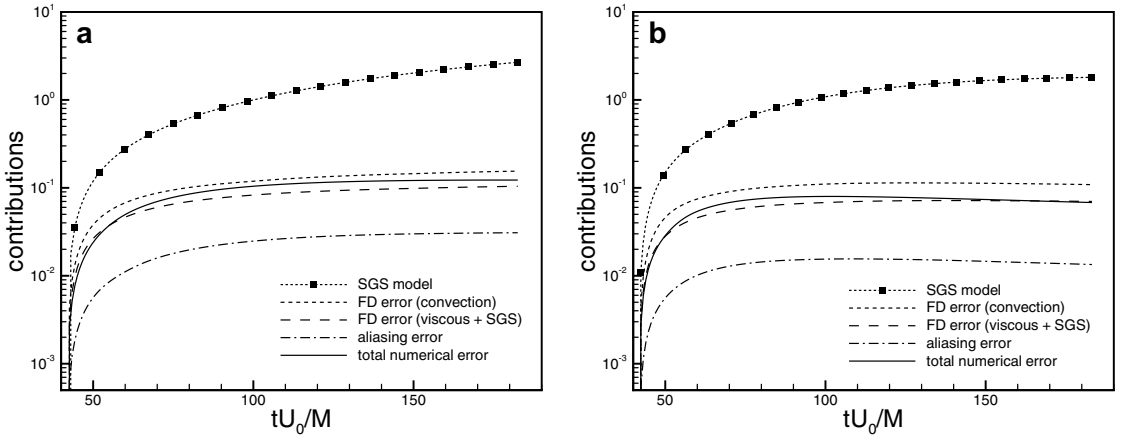

Fig. 11. Contribution of SGS model and numerical errors on the solution evolution of CBC-isotropic turbulence: (a) $k_c = 16$; (b) $k_c = 32$.

error in the convection term. Consequently, total error defined by (59) is smaller than the error due to the convection term alone. Also note that aliasing error is a negligible source of the numerical error; it is about 1% of resolved kinetic energy, consistent with results in Section 3.

In order to generalize the above conclusion, we consider isotropic turbulence at much higher Reynolds number of $Re_\lambda = 10^4$, initialized by the Gaussian energy spectrum

$$E(k,0) = \left(16\sqrt{\frac{2}{\pi}u_0^2/k_p^5}\right)k^4 \exp(-2k^2/k_p^2), \tag{60}$$

where $u_0 = 1$ and $k_p = 5$. Temporal evolutions of the contributions of numerical error and SGS model for $k_c = 32$ are shown in Fig. 12(a). The behavior is essentially the same as that observed for CBC-isotropic turbulence in Fig. 11. The main difference is that the finite-differencing error is larger than the SGS contribution in the initial stage. However, this only reflects the fact that there is negligible energy at high wavenumbers of the initial spectrum (60), and therefore the SGS term, viscous error term and aliasing error are not activated. Only after two eddy turn-over time t_e, the SGS contribution starts dominating other numerical errors and its contribution grows in time to reach 10 times of resolved kinetic energy.

From Figs. 11 and 12(a), it seems that the temporal variation of contributions are small except the SGS contribution, which continuously grows in time. Thus, it is reasonable to consider the time average of the contribution defined, for example, by $\bar{\sigma}^{\mathrm{SGS}} = \frac{1}{(T-t_0)}\int_{t_0}^{T}\sigma^{\mathrm{SGS}}(t)\,\mathrm{d}t$. Such averaged contributions for the isotropic turbulence of $Re_\lambda = 10^4$ at five ($k_c = 8$, 16, 32, 64 and 128) cutoff wavenumbers are shown in Fig. 12(b). Note that all cutoff wavenumbers belong to the inertial range and that five independent EDQNM-LES are performed at each cutoff wavenumber to construct data to plot Fig. 12(b). To remove the initial condition effect, $t_0 = 4t_e$ is used. It is clear that the SGS contribution dominates the numerical errors at all filter sizes, when the cutoff lies in the inertial range.

As a summary of the error estimation in this section, we note that the numerical error of SCD2 in LES is responsible for approximately 10% of resolved kinetic energy for flows at sufficiently high Reynolds numbers, whereas the solution is entirely dependent upon SGS model because its absence results in unacceptable solution.

5. Static vs. dynamic error analysis

5.1. The static error analysis

The Navier–Stokes counterpart of (58) takes the following form:

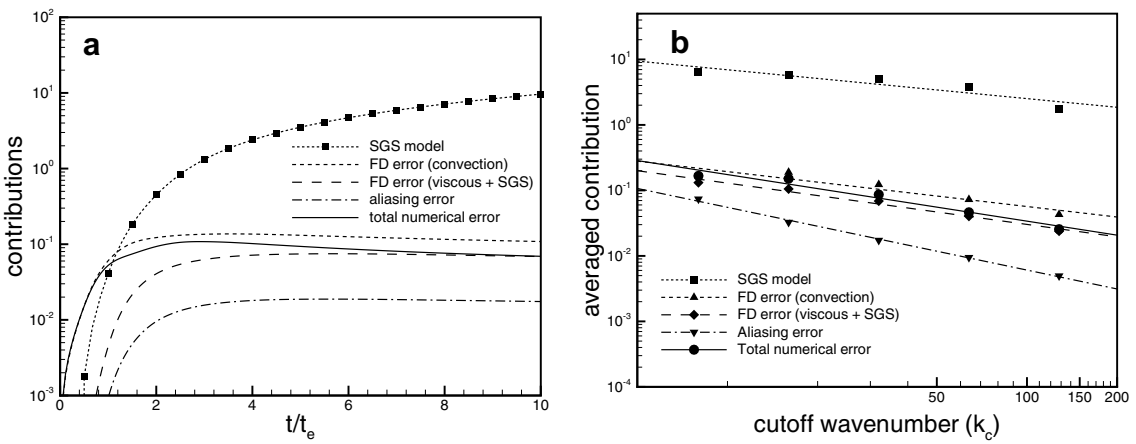

Fig. 12. Contribution of SGS model numerical errors for LES of the isotropic turbulence at $Re_\lambda = 10^4$ with second-order central difference code: (a) temporal evolution of contributions at $k_c = 32$; (b) averaged contribution at several cutoff wavenumbers (lines denote the least-square fit.).

$$\frac{\partial\hat{v}(\mathbf{k},t)}{\partial t} = -\mathrm{i}P_{imn}(\mathbf{k}')H(\mathbf{k})\left[\sum_{\mathbf{a}\in\Lambda} d\mathbf{q}\delta(\mathbf{p}+\mathbf{q}-\mathbf{k}-\mathbf{a})\hat{v}_m(\mathbf{p},t)k_a^1(\mathbf{p})\hat{v}_n(\mathbf{q},t)k_a^2(\mathbf{q})\right] - \nu k''\hat{v}_i(\mathbf{k},t) - \mathrm{i}P_{imn}(\mathbf{k}')\hat{\tau}^{\mathrm{M}}_{mn}(\mathbf{k}',t). \tag{61}$$

When $v_i(\mathbf{x},t)$ is initialized by $v_i(\mathbf{x},t_0)=\bar{u}_i(\mathbf{x},t_0)$, it will deviate from $\bar{u}_i$ at a rate proportional to the magnitude of the numerical errors. The numerical error may be considered the origin of this deviation. Ghosal [6] defines the error by the difference between terms on the right-hand side of (19) and (61). This definition is valid under the condition of $v_i=\bar{u}_i$, which is satisfied at $t=t_0$. Then, the numerical errors $E_i(\mathbf{k})=E_i^{(\mathrm{FD})}(\mathbf{k})+E_i^{(\mathrm{alias})}(\mathbf{k})$ are

$$E_i^{(\mathrm{FD})}(\mathbf{k}) = \mathrm{i}H(\mathbf{k})[P_{imn}(\mathbf{k}')-P_{imn}(\mathbf{k})]\left[\int_{\square}\int_{\square}\mathrm{d}^3\mathbf{p}\,\mathrm{d}^3\mathbf{q}\delta(\mathbf{p}+\mathbf{q}-\mathbf{k})\hat{\bar{u}}_m(\mathbf{p})\hat{\bar{u}}_n(\mathbf{q})+\hat{\tau}^{\mathrm{M}}_{mn}(\mathbf{k})\right]+\nu(k''-k^2)\hat{\bar{u}}_i(\mathbf{k}), \tag{62}$$

$$E_i^{(\mathrm{alias})}(\mathbf{k}) = \mathrm{i}P_{imn}(\mathbf{k}')H(\mathbf{k})\sum_{\mathbf{a}\in\Lambda_0}\left[\int_{\square}\int_{\square}\mathrm{d}^3\mathbf{p}\,\mathrm{d}^3\mathbf{q}(\mathbf{q})\delta(\mathbf{p}+\mathbf{q}-\mathbf{k}-\mathbf{a})\hat{\bar{u}}_m(\mathbf{p})\hat{\bar{u}}_n\right], \tag{63}$$

where $E_i^{(\mathrm{FD})}(\mathbf{k})$ and $E_i^{(\mathrm{alias})}(\mathbf{k})$ respectively denotes the finite-differencing and aliasing error. For simplicity, $k_a^1=k_a^2=1$ is assumed in (62) and (63) following Ghosal [6], which means that only the divergence form of the nonlinear term on the regular mesh is considered. Then, these errors are characterized by the power spectral densities (PSDs) of the form

$$\epsilon^{\mathrm{FD}}(k) = 4\pi k^2\lim_{L\to\infty}\frac{8\pi^3}{L^3}\left\langle E_i^{(\mathrm{FD})}(\mathbf{k})\cdot E_i^{(\mathrm{FD})}(\mathbf{k})^*\right\rangle_k, \tag{64}$$

where $\langle\,\rangle_k$ denotes the ensemble and spherical shell average at $k=|\mathbf{k}|$. PSD of aliasing error and true SGS force also takes the same form. Quadruple nonlinear terms that appear in PSDs are closed by using the joint normal hypothesis [13] given by Eq. (7) to get their analytic expressions. By ignoring the viscous term, these PSDs can be computed once the three-dimensional energy spectrum $E(k)$ and modified wavenumbers are given. Then, the "static error analysis" is performed in terms of PSDs of numerical errors and SGS force.

For the compatibility of the dynamic error analysis in Section 4 with CBC-isotropic turbulence, the static error analysis is performed on the CBC-isotropic turbulence at the initial stage of $tU_0/M=42$ as shown in Fig. 13. Here, the second-order central difference with divergence-form of nonlinear term is considered at $k_c=16$ and 64. As shown in Fig. 13, the results are essentially the same with those from the von Kármán spectrum [6] in that both the power spectral densities of finite-differencing and aliasing errors overwhelm that of SGS force nearly at all wavenumbers. By approximating integration within the domain $\square$ in terms of two spherical domains, lower and upper bounds for SGS force and aliasing error are introduced [6]. Since the present cutoff filter corresponds to the inner sphere, the upper bound of SGS force and lower bound of the aliasing error should be selected. Although this reduces the gap between SGS force and numerical error, this still does not change the conclusion of the static error analysis. Especially, it is remarkable that even the lower bound of the aliasing error is comparable to SGS force at all wavenumbers. These results clearly contradict those obtained from dynamic error analysis and actual LES in Section 4. The following section attempts to explain this discrepancy.

5.2. A critical look at the static error analysis

Based on the present results, we suggest the following four limitations of the static error analysis.

- Fully-coupled nature between numerical error and solution

The PSDs are not functions of energy spectrum when $v_i(\mathbf{x},t)\neq\bar{u}_i(\mathbf{x},t)$, which is true for all $t>t_0$. In this case, difference between terms on the r.h.s of (19) and (61) becomes a complex expression such that its PSD cannot be analytically computed with statistical closure theories. Sharing the same symbol, the difference between the reference $\bar{u}_i$ and numerical solution v_i is often overlooked when numerical error is defined. The

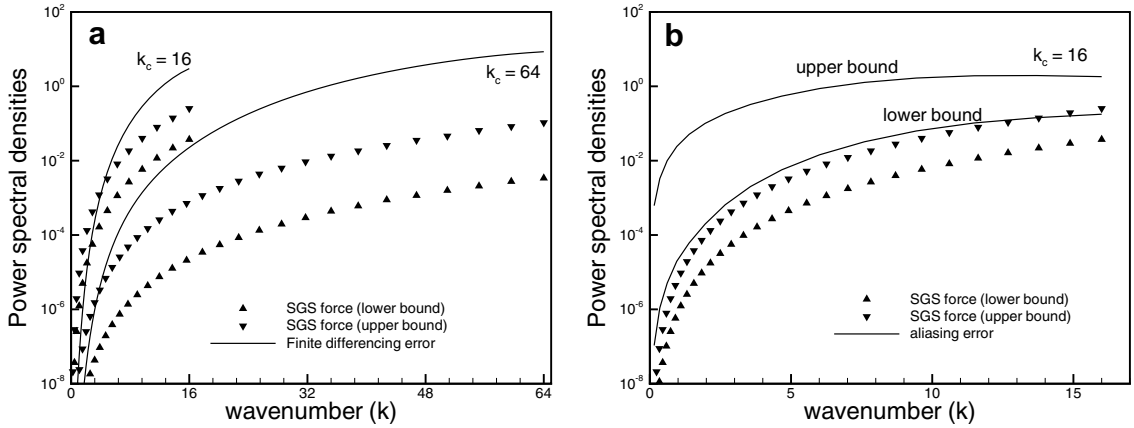

Fig. 13. The "static" (a) finite-differencing and (b) aliasing errors for second-order central difference scheme compared with lower and upper bounds for SGS force for the initial spectrum of CBC-isotropic turbulence at $tU_0/M = 42$.

numerical error defined in this manner only reflects the deviation from the exact solution at any given instant, and thus the cumulative nature of error cannot be accounted. Tracing the contribution of numerical error on the solution appears more preferable.

- Positive nature of the power spectral density

In the static error analysis, the magnitude of errors are quantified by the power spectral density (PSD). The PSD is probably not the best measure to quantify errors in the dynamic system. The "positive nature" of PSD can cause the overprediction of numerical error and misleading conjectures. For example, Park et al. [12] show that PSD of the aliasing error for upwind scheme is larger than that of comparable central difference schemes. This result is obviously wrong because numerical dissipation embedded in upwind schemes actually reduces aliasing error, while the imaginary part of modified wavenumber of such schemes increase PSD of aliasing error. It is informative to analyze terms in (58) in the form of

$$\left.\frac{\partial \overline{E}(k)}{\partial t}\right|_{t=t_0} = \int\int_{\Delta'_k} \mathscr{I}\,\mathrm{d}p\,\mathrm{d}q - 2(\nu+\nu_T)k^2\overline{E}(k) + T^{\mathrm{FD}}(k) + T^{\mathrm{alias}}(k), \tag{65}$$

$$T^{\mathrm{FD}}(k) = \int\int_{\Delta'_k} \left(A(p)A(q)\mathscr{I}^{\mathrm{CD2}}(k,k',p,q) - \mathscr{I}(k,p,q)\right)\mathrm{d}p\,\mathrm{d}q + 2\left(-\nu(k''^2_{3\mathrm{D}} - k^2) - \nu_T^{\mathrm{CD2}}k''^2_{3\mathrm{D}} - \nu_T k^2\right)\overline{E}(k), \tag{66}$$

$$T^{\mathrm{alias}}(k) = \left\{\sum_{\mathbf{a}\in\Lambda_0}\left[\int\int_{\Delta_{|\mathbf{k}+\mathbf{a}|}} \frac{kA(p)A(q)}{|\mathbf{k}+\mathbf{a}|}\mathscr{I}^{\mathrm{CD2}}(k,k',p,q)\,\mathrm{d}p\,\mathrm{d}q\right]\right\}_k, \tag{67}$$

where terms on the r.h.s. of (65) respectively denote the resolved nonlinear term, viscous and SGS term, finite-differencing error and aliasing error. Note that the exact form of aliasing error given by (54) is considered. These five terms for CBC-isotropic turbulence at the initial state ($tU_0/M = 42$) are shown in Fig. 14. As discussed above, the error transfer term $T^{\mathrm{FD}}(k)$ and $T^{\mathrm{alias}}(k)$ are meaningful only when $t = t_0$ or $\overline{E}(k) = E^{\mathrm{CD2}}(k)$. From Fig. 14, it is again clear that numerical errors are smaller than SGS contribution and this is especially true for the aliasing error. More importantly, the transfer functions of numerical errors and that of SGS model are of opposite sign. Furthermore, SGS term is the only element that gives the dissipation at high wavenumbers since the viscous term is negligible at this resolution ($k_c = 16$). Thus, it is easy to imagine the extreme pile-up of energy would happen to the solution in the absence of SGS term as shown in Fig. 4. From Fig. 14, it appears important that a quantitative estimate of numerical error or SGS force needs to determine if the error is a source or a sink for the system. The PSD does not provide this information.

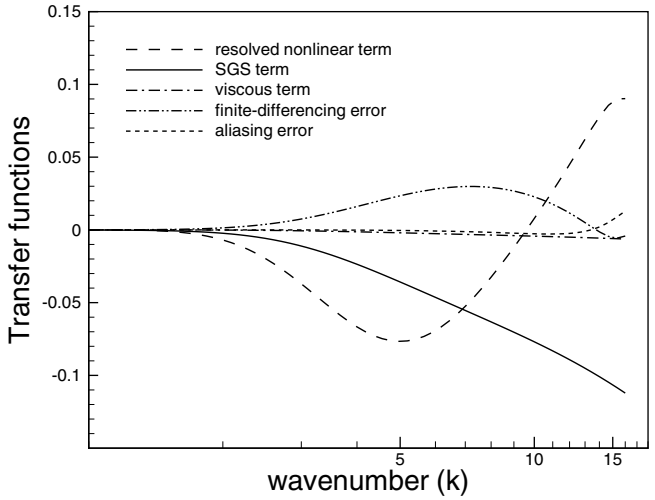

Fig. 14. Spectral contributions of terms in a EDQNM-LES (the model of second order LES code) for the initial spectrum of CBC-isotropic turbulence at $tU_0/M = 42$.

- Interaction between SGS model and numerical error

Next, the interaction between SGS model and numerical error can be considered as a time-stepping effect, that is neglected in the static error analysis. One may argue that the sensitivity of DSM to numerical error is evidence that numerical error corrupts the SGS model, but this sensitivity appears to be a welcome feature of DSM. Consider Fig. 15, where $\overline{E}(k)$ (reference) and $E^{v}(k)$ (denoted as RUN1) with 5pt-stencil scheme for the viscous term (See Section 3) are plotted at $tU_0/M = 171$ together with the evolution of corresponding Smagorinsky constant C_s. Note that the large pile-up at high wavenumber due to finite-differencing error has resulted in a significant increase of C_s. From a simple numerical test, one can see that the result would be even worse if C_s did not increase. To verify this argument, RUN2, a similar simulation to RUN1 except that C_s from the reference simulation is prescribed, is conducted. As can be readily imagined, RUN2 shows severe pile-up of

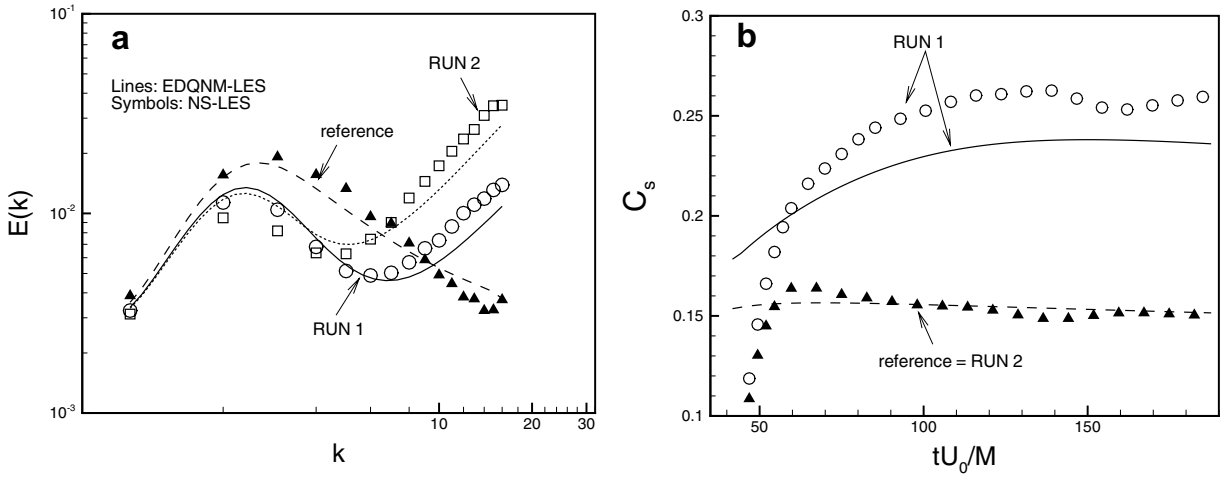

Fig. 15. Interaction between SGS model and numerical error: (a) energy spectra of CBC-isotropic turbulence at $tU_0/M = 171$; (b) evolutions of the dynamic Smagorinsky constant C_s. Here, reference denotes dealiased spectral method and RUN1 corresponds to LES with 5-pt second stencil order central difference for viscous terms described in Section 3.2. RUN2 is the same with RUN1 except that the dynamic constant is prescribed as that obtained from the reference simulation.

energy. This is due to the dynamic adjustment mechanism of DSM to keep the equilibrium of SGS dissipation [12], which should be taken into consideration in error analysis.

- divergence-form of the nonlinear term

Finally, the use of the divergence-form of the nonlinear term for the static error analysis needs to be considered. It is well known that the skew-symmetric form or staggered approach predicts smaller finite-differencing and aliasing error [7,12] than divergence form. Besides, the use of divergence form cannot give stable solution in the actual turbulence simulation due to the violation of kinetic energy conservation [7,29], and therefore should not be considered, even in the theoretical analysis.

6. Concluding remarks

A dynamic theory is developed to predict the impact of numerical error in solutions to the LES equations for isotropic turbulence. Kinetic energy evolution equation in the wavespace is considered, and the evolution equation for the energy spectrum is closed by EDQNM theory. Finite differencing error, aliasing error and dynamic Smagorinsky model for the energy-conserving second order central difference scheme are incorporated in this one-dimensional equation using the notion of modified wavenumber. The resulting model predictions are compared to solutions from actual three-dimensional LES, where the same errors are introduced. It is shown that the proposed model equation is capable of reproducing actual LES results.

The model equation is used to perform a dynamic error analysis for the decaying isotropic turbulence of Comte-Bellot and Corrsin [23]. The contributions of numerical error and SGS term on the solution are evaluated. This analysis shows that the contribution of SGS model to LES solution is much more significant that those of finite-differencing and aliasing errors for LES with energy-conserving second order central difference scheme. The analysis of energy transfer shows that numerical errors result in the injection of energy at intermediate wavenumbers, whereas the transport of SGS term indicates a large drain, or the forward transfer, of the energy having the peak at the cutoff. Therefore, numerical error cannot mask SGS contribution on the solution, at least for isotropic turbulence, and the non-dissipative numerical method considered.

The present conclusions strictly hold for isotropic turbulence. Complex inhomogeneous flows involve sources of numerical errors which were not considered in this paper such as the grid non-uniformity, mesh skewness, smooth filter and boundary conditions. Finally, note that the one-dimensional EDQNM-LES model introduced in the present study can be a more general tool for the analysis of numerical error and the performance of SGS model in turbulence simulations.

Acknowledgments

This work was supported by the Department of Energy under the Stanford ASC alliance, and the Air Force Office of Scientific Research under grant FA9550-04-1-0341. Computer time was provided by the Minnesota Supercomputing Institute, the San Diego Supercomputer Center, and the National Center for Supercomputing Applications.

Appendix A. Note on conservation properties

Discrete conservation of kinetic energy allows non-dissipative schemes to be stable at high Reynolds numbers. For Fourier spectral methods, the skew-symmetric form of the convection term conserves kinetic energy in the presence of aliasing error. Other forms (divergence and advection) are conservative only when aliasing error is absent [7]. For second-order central differences, the skew-symmetric form on a regular mesh, and divergence form on a staggered mesh conserve kinetic energy even in the presence of aliasing error [7].

It is difficult to represent local conservation of kinetic energy in the framework of EDQNM-LES. Instead, global conservation of total kinetic energy can be investigated by checking the symmetry $\sum \mathscr{I} = \mathscr{I}(k,p,q) + \mathscr{I}(p,q,k) + \mathscr{I}(q,k,p) = 0$ [19]. This takes the form

$$\sum \mathscr{I} = C_1 \cdot E(p)E(q)\frac{k}{pq} + C_2 \cdot E(q)E(k)\frac{p}{qk} + C_3 \cdot E(k)E(p)\frac{q}{kp}, \tag{68}$$

$$\begin{aligned} C_1(\mathbf{k},\mathbf{p},\mathbf{q}) &= J_1(\mathbf{k},\mathbf{p},\mathbf{q}) + J_3(\mathbf{q},\mathbf{k},\mathbf{p}) + J_2(\mathbf{p},\mathbf{q},\mathbf{k}), \\ C_2(\mathbf{k},\mathbf{p},\mathbf{q}) &= J_3(\mathbf{k},\mathbf{p},\mathbf{q}) + J_2(\mathbf{q},\mathbf{k},\mathbf{p}) + J_1(\mathbf{p},\mathbf{q},\mathbf{k}), \\ C_3(\mathbf{k},\mathbf{p},\mathbf{q}) &= J_2(\mathbf{k},\mathbf{p},\mathbf{q}) + J_1(\mathbf{q},\mathbf{k},\mathbf{p}) + J_3(\mathbf{p},\mathbf{q},\mathbf{k}). \end{aligned} \tag{69}$$

For the Fourier spectral method, $\sum \mathscr{I} = 0$ is automatically satisfied, since $C_1 = C_2 = C_3 = 0$ due to symmetry. However, note that $\sum \mathscr{I} = 0$ even in the presence of aliasing error aliasing error (53); an aliased spectral method in divergence form therefore conserves kinetic energy for EDQNM-LES. Fig. 16(a) shows kinetic energy evolution in the inviscid limit for CBC-isotropic turbulence. From Fig. 16(a), an aliased spectral method rapidly diverges in the actual Navier–Stokes simulation, whereas EDQNM simulation exactly conserves kinetic energy. This explains the discrepancy of energy spectra between EDQNM-LES and NS-LES shown in Fig. 9(a).

For finite-difference schemes with divergence form, it is easy to show $C_1 = J_1'(\mathbf{k},\mathbf{k}',\mathbf{p},\mathbf{q}) + J_2'(\mathbf{q},\mathbf{q}',\mathbf{k},\mathbf{p}) + J_3'(\mathbf{p},\mathbf{p}',\mathbf{q},\mathbf{k}) \neq 0$ due to asymmetry. Similarly, $C_2 \neq 0$ and $C_3 \neq 0$ for these cases. Thus, in general $\sum \mathscr{I} \neq 0$ for finite-difference schemes. From numerical experiments, it is found that this error is dissipative in EDQNM-LES. This is contrary to the conservation error of NS-LES that causes the solution to diverge (see Fig. 16(a)). Note that there is no aliasing error in this simulation. Thus, the conservation error is part of the finite-differencing error in this case.

It is illustrative to compare $E^c(k,t)$ from EDQNM-LES and NS-LES, for the divergence-form, second order central difference scheme as shown in Fig. 16(b). The agreement between two spectra is good up to $k = 10$, but they show large deviation at higher wavenumbers. If there were no conservation error, the correct spectrum should resemble that from the EDQNM-LES, since the nonlinear transfer term goes to zero at the cutoff, due to the modified wavenumber. Only viscous and SGS terms are significant near the cut-off. Consistent with our conjecture in Section 3, conservation error occurs at the smallest scale due to violation of local conservation property. Morinishi et al. [29] show that the conservation error at each node is $-u_j u_i(\delta_2 u_i/\delta_2 x_j)$ for the divergence form CD2. It might be desirable to somehow model this effect in EDQNM closure; however, such modification was not pursued in this study.

On the other hand, it is found from numerical experiments that the approximation of staggered second order central difference scheme (SCD2), Eq. (39), result in $\sum \mathscr{I} = 0$ although C_i's are nonzero. However,

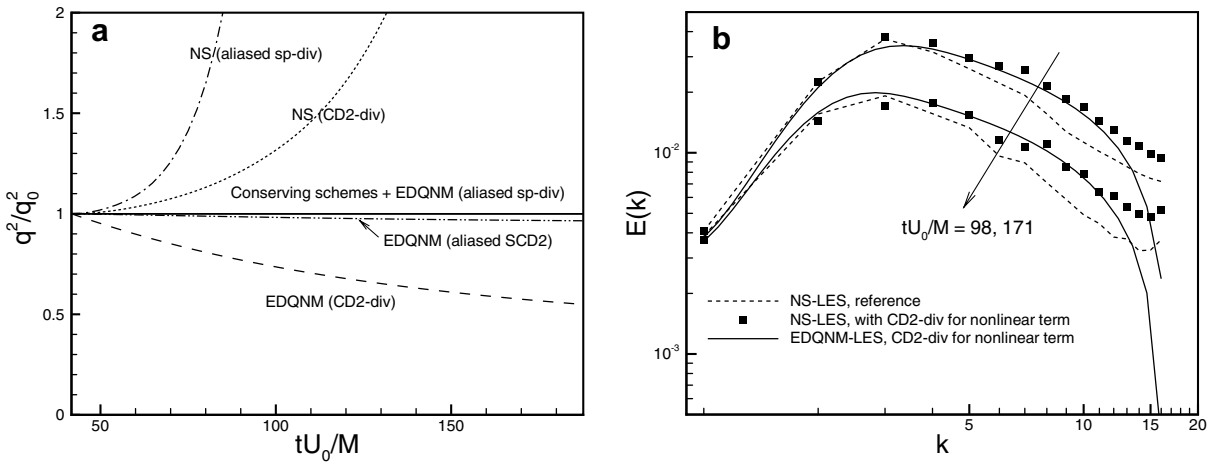

Fig. 16. Conservation property of various schemes and impact of the conservation error on the energy spectra: (a) time evolution of total kinetic energy in the inviscid limit. Here, sp-div and CD2-div respectively denote the spectral and second-order central difference method with divergence form nonlinear term. Conserving schemes include dealiased spectral method, spectral method with skew-symmetric form, and staggered second-order central difference with and without aliasing error (for both EDQNM and NS simulation). (b) energy spectra for CBC-isotropic turbulence with CD2-div from NS-LES and EDQNM-LES.

the aliasing error introduces a small dissipation as shown in Fig. 16(a). Since this error is very small, it does not affect the overall accuracy of the simulation. Therefore, as far as SCD2 is concerned, both NS-LES and EDQNM-LES show good conservation property. This property serves as the basis of the good agreement between EDQNM-LES and NS-LES shown in Sections 3 and 4.

References

[1] C. Meneveau, J. Katz, Scale-invariance and turbulence models for large-eddy simulation, Annu. Rev. Fluid Mech. 32 (2000) 1.
[2] P. Moin, Advances in large eddy simulation methodology for complex flows, Int. J. Heat Fluid Flow 23 (2002) 710.
[3] P. Sagaut, Large Eddy Simulation for Incompressible Flows, second ed., Springer-Verlag, 2002.
[4] P. Beudan, P. Moin, Numerical experiments on the flow past a circular cylinder at a sub-critical Reynolds number, Report No. TF-62, Dept. Mech. Eng., Stanford University, 1994.
[5] R. Mittal, P. Moin, Suitability of upwind-biased finite-difference schemes for large-eddy simulation of turbulent flows, AIAA J. 35 (1997) 1415.
[6] S. Ghosal, An analysis of numerical errors in large-eddy simulations of turbulence, J. Comput. Phys. 125 (1996) 187.
[7] G. Kravchenko, P. Moin, On the effect of numerical errors in large-eddy simulations of turbulent flows, J. Comput. Phys. 131 (1997) 310.
[8] T.S. Lund, The use of explicit filters in large eddy simulation, Comput. Math. Appl. 46 (2003) 603.
[9] I. Fedoiun, N. Lardjane, I. Gokalp, Revisiting numerical errors in direct and large eddy simulations of turbulence: physical and spectral space analysis, J. Comput. Phys. 174 (2001) 816.
[10] J. Gullbrand, F.K. Chow, The effect of numerical errors, turbulence models in LES of turbulent channel flow, with and without explicit filtering, J. Fluid Mech. 495 (2003) 323.
[11] F.K. Chow, P. Moin, A further study of numerical errors in large-eddy simulations, J. Comput. Phys. 184 (2003) 366.
[12] N. Park, J.Y. Yoo, H. Choi, Discretization errors in large eddy simulation: on the suitability of centered and upwind-biased compact difference schemes, J. Comput. Phys. 198 (2004) 580.
[13] A. Monin, A. YaglomStatistical Fluid Mechanics, vol. 2, MIT Press, Cambridge, MA, 1979.
[14] K. Akselvoll, P. Moin, Large-eddy simulation of turbulent confined coannular jets, J. Fluid Mech. 315 (1996) 387.
[15] B. Vreman, B. Geurts, H. Kuerten, Large eddy simulation of the turbulent mixing layer, J. Fluid Mech. 339 (1997) 357.
[16] K. Mahesh, G. Constantinescu, P. Moin, A numerical method for large eddy simulation in complex geometries, J. Comput. Phys. 197 (2004) 215.
[17] R.H. Kraichnan, Convergents to turbulence functions, J. Fluid Mech. 41 (1970) 189.
[18] M. Lesieur, Turbulence in Fluids, Kluwer Academics, Dordrecht, 1987.
[19] D.C. Leslie, Developments in the Theory of Turbulence, Oxford University Press, Oxford, 1973.
[20] S.A. Orszag, Analytical theories of turbulence, J. Fluid Mech. 41 (1970) 363.
[21] C.E. Leith, Atmospheric predictability and two-dimensional turbulence, J. Atmos. Sci. 28 (1971) 145.
[22] P. Moin, Fundamentals of Engineering Numerical Analysis, Cambridge University Press, 2001.
[23] G. Comte-Bellot, S. Corrsin, Simple Eulerian time correlation of full- and narrow-band velocity signals in grid-generated, 'isotropic' turbulence, J. Fluid Mech. 48 (1971) 273.
[24] M. Germano, U. Piomelli, P. Moin, W. Cabot, A dynamic subgrid-scale eddy viscosity model, Phys. Fluids A 3 (1991) 1760.
[25] R. Akhavan, A. Ansari, S. Kang, N. Mangiavachi, Subgrid-scale interactions in a numerically simulated planar turbulent jet and implications for modelling, J. Fluid Mech. 408 (2000) 83.
[26] N. Park, J.Y. Yoo, H. Choi, Toward improved consistency of a priori tests with a posteriori tests in large eddy simulation, Phys. Fluids 17 (2005) 015103.
[27] J.P. Chollet, Two-point closure used for a sub-grid scale model in large eddy simulations, in: L.J.S. Bradbury et al. (Eds.), Turbulent Shear Flows, vol. 4, Springer, 1985, p. 66.
[28] D. Lilly, A proposed modification of the Germano subgrid scale closure method, Phys. Fluids A 4 (1992) 633.
[29] Y. Morinishi, T.S. Lund, O.V. Vasilyev, P. Moin, Fully conservative higher order finite difference schemes for incompressible flow, J. Comput. Phys. 143 (1998) 90.
[30] F. Ducros, F. Laporte, T. Souleres, V. Guinot, P. Moinat, B. Caruelle, High-order fluxes for conservative skew-symmetric-like schemes in structured meshes: application to compressible flows, J. Comput. Phys. 161 (2000) 114.
[31] M.R. Visbal, D.V. Gaitonde, High-order accurate methods for complex unsteady subsonic flows, AIAA J. 37 (10) (1999) 1231.